*J. Fluid Mech.* (1987), *vol.* 181, *pp.* 163–195
*Printed in Great Britain*



# On the computation of transonic leading-edge vortices using the Euler equations

By ARTHUR RIZZI

FFA, The Aeronautical Research Institute of Sweden, S-161 11 Bromma, Sweden
and Royal Institute of Technology, S-100 44 Stockholm, Sweden

AND CHARLES J. PURCELL

ETA Systems, Inc., St Paul, MN 55108, USA

(Received 29 November 1985 and in revised form 6 November 1986)

Separation from the leading edge of a delta wing with the subsequent roll-up into a vortex has been simulated in numerical solutions to the Euler equations. Such simulations raise a number of questions that are still outstanding, including the process of inviscid separation from a smooth edge, the role of artificial viscosity in the creation and capturing of vortex sheets, the roll-up mechanism and core features, losses in total pressure, and the stability of the vortical flow structures to three-dimensional disturbances. These matters are discussed in the context of two numerical experiments, both carried out in a sequence of three simulations that starts with a coarse-mesh discretization and ends with a fine mesh of over one million cells. The first experiment is for transonic flow, $M_\infty = 0.7$, $\alpha = 10°$, around a pure delta wing. The sequence converges to the expected classical steady vortex flow. In the second experiment, transonic flow, $M_\infty = 0.9$, $\alpha = 8°$, past a twisted cranked-and-cropped delta wing, the sequence does not converge. Instead the crank is observed in the fine-mesh solution to set off an instability in the vortex sheet that causes the vortex to burst into a thin chaotic vortical layer embedded in laminar flow. The mesh sequence suggests that it is the shortest waves resolved that are most unstable, but the energy contained in them comes from the large-scale motion and seems to be small.

## 1. Introduction

Vortex flows are among the most difficult to analyse because of their inherently nonlinear interactions. In order to reach a better understanding one therefore tries to study a model problem that contains only one generic aspect of such flows in a simple setting, free of other complications. But it is not easy to find a simple two-dimensional model problem of vortex flow, preferably with an analytic solution, because many of these are often time dependent and even unstable. One inviscid model, however, of steady flow past a slender conical delta wing of infinite length in which a vortex is shed from the leading edge has been studied numerically and has offered insight into the nature of the problem (see the two recent reviews by Hoeijmakers 1984 and Smith 1984 and the references therein). The vortex in reality is formed by the rolling up of the shed shear layer. In the limit of the vanishing viscosity of the theoretical model the shear layer shrinks in thickness to a vortex sheet, which coils up into a spiral having an infinite number of turns. Actually a vortex core never forms at the centre of this theoretical inviscid spiral, and hence

this model is unrealistic in terms of detailed core structure, which is a viscous phenomenon. In practical computations, at most only a few turns of the coil are accurately resolved before the structure of the spiral is either lost in the dissipation inherent in a finite representation, or is replaced by another model for the core, e.g. a line vortex. In either case an accurate and detailed representation of the core structure is doubtful. But just outside the core the model does represent accurately the global quantities like circulation around the core. And the vortex sheet is the appropriate model to study the dynamics and stability of the roll-up process, since its inflexional velocity profile suggests that an instability would be inviscid in nature. Although one might expect a Rayleigh instability, Moore & Griffith-Jones (1974) and Moore (1973), making the two-dimensional time-dependent analogy, have analysed the problem of the coiling sheet and found it to be marginally stable to two-dimensional disturbances, the shortest wavelengths being the least stable†. The stretching of the sheet as it winds into the spiral is the stabilizing process. In three dimensions, only computational models have been formulated to study the corresponding problem where the wing is given a trailing edge and so truncated to a finite length. If the flow is subsonic, the problem cannot be strictly conical. The upwash at the trailing edge then produces a three-dimensional disturbance that makes the flow locally non-conical, but a number of numerical computations (Hoeijmakers & Vaatstra 1983; Krause, Shi & Hartwich 1983; Rizzi & Eriksson 1985; Rizzi 1985*a*) indicate that the resulting sheet structure still remains stable even in very high-resolution simulations that represent the small-scale modes well (Rizzi 1985*b*). Evidently the disturbance of the trailing edge is not great enough to upset stability in these particular cases. Flows such as these, we believe, can be characterized as being of low helicity and are relatively stable because they are primarily two-dimensional in structure.

The question we wish to raise here is: what happens to stability if the wing configuration is fundamentally non-conical and the flow is high speed and compressible? A good example of this is a wing with a cranked delta planform, which is currently attracting considerable practical interest. In general the flow field can be thought of as one with high helicity. At some angle of attack a vortex sheet is shed from the leading edge, but the precise dynamics of the sheet are not well understood. For example, whether one single contiguous sheet is shed along the entire leading edge; or whether two distinct vortices form; and under what conditions the vortical features remain stable, are still open questions. We intend, therefore, to explore this issue in the thrust of a numerical experiment offering high resolution, with the hope of providing at least some preliminary insight into the nature of this flow and the behaviour of the computational model based on the Euler equations of motion.

Two flows are studied under the same conditions of the numerical experiment. The first is the classical and better understood problem of flow past a pure delta wing that is flat and of zero thickness, and serves as the control case. The second geometry is a cranked delta with finite thickness and twist. Our intention is to observe the gross effects of these two different geometries, with the hope that the contrast in results

† Whether the vortex sheet is judged either marginally stable or marginally unstable depends on the adopted criterion for stability, in particular the norm chosen to measure the growth and determine the bound. Our purposes here do not warrant a technical discussion of this issue. A remark of Moore & Griffith-Jones (1974) is relevant, however: 'even in a case where the flow is stable according to [Moore's] criterion, a disturbance of short wavelength can undergo considerable amplification even though its amplitude remains bounded as $t \to \infty$'.

will shed some light on the dynamics of leading-edge vortices as represented in numerical solutions to the Euler equations.

Designed to gauge the effect of the mesh size, the experiment consists of a series of three simulations, for each of the two cases, with progressively finer meshes. As the mesh size decreases, the resolution of the results improves, and thus the comparison of the three computations enables us to judge the behaviour of the large-scale modes separately from that of the small-scale ones. For the pure delta we find only small changes in the solution obtained on the fine mesh compared with that on the medium mesh. This indicates a convergence with mesh size and a reasonably accurate solution. It also suggests that the solution consists almost entirely of large-scale modes that are well represented on the medium mesh. This observation stands in contrast to the results for the cranked delta. We find here that in the coarse-mesh solution, the flow is laminar and contains only stable long modes. Shorter modes enter in the medium-mesh results that begin to indicate a wavelike character, while the shortest scales on the fine mesh show a very chaotic pattern, superimposed upon the coarser laminar field, in a thin layer over the wing outboard of the crank. The reason for this, we believe, is the strong spanwise flow set in motion by the lower sweep angle outboard which generates substantial shear. This thin layer of high shear seems to be unstable so that as the mesh is refined smaller-scale modes continually appear.

At this time it is not at all certain that flow instabilities can be studied by numerical solutions calculated on a finite grid. Indeed there are still a number of outstanding questions about whether the Euler equations are in fact the appropriate model for shed-vortex flow, particularly if the shedding edge is round. But our dense-mesh solutions do contain some degree of similarity to how we think these flows actually behave. In this regard, our knowledge of these particular cases is somewhat more limited because of the difficulty in carrying out physical measurements of transonic vortex flow in a wind tunnel. It is in this spirit then that we present our numerical observations in order to continue the current debate about Euler computations for vortex flow in general, and specifically to bring to light the possibility of vortical instabilities brought about by the geometry of the wing form.

## 2. Numerical solution procedure

Rizzi & Eriksson (1984) describe the numerical method that we use to solve the Euler equations. In this finite-volume procedure the Euler equations for compressible flow are expressed as the integral balance of the conservation laws

$$\frac{\partial}{\partial t}\iiint \boldsymbol{q}\,\mathrm{dvol} + \iint \boldsymbol{H}(\boldsymbol{q})\cdot\boldsymbol{n}\,\mathrm{d}s = 0, \tag{1}$$

where $\boldsymbol{q}$ is the vector with elements of mass and momentum. Since the total enthalpy $h_0$ in the steady flows under consideration here is constant, the energy equation is not needed in the system. The inviscid flux quantity $\boldsymbol{H}(\boldsymbol{q})\cdot\boldsymbol{n}$ represents the net flux of $\boldsymbol{q}$ transported across, plus the pressure $p$ acting on, the surface $S$ surrounding the volume of fluid. The method adds another term $Y$ to (1), an artificial viscosity model of the form

$$Y(\boldsymbol{q}) = \chi[\delta_I s_I(p)\,\delta_I + \delta_J s_J(p)\,\delta_J + \delta_K s_K(p)\,\delta_K]\,\boldsymbol{q} - A(\delta_I^4 + \delta_J^4 + \delta_K^4)\,\boldsymbol{q}.$$

It has the property of an energy sink for the shortest modes, i.e. $(\mathrm{d}/\mathrm{d}t)\,q^2 < 0$ summed over all the cells including those at the boundaries. It makes the method dissipative.

The finite-volume scheme then discretizes (1) by assuming that $\boldsymbol{q}$ is a cell-averaged quantity located in the centre of the cell, and the flux term $\boldsymbol{H}(\boldsymbol{q})\cdot\boldsymbol{n}$ is defined only at the cell faces by averaging the values on each side. With these definitions, and calling the cell surfaces in the three coordinate directions of the mesh $\boldsymbol{S}_I$, $\boldsymbol{S}_J$, and $\boldsymbol{S}_K$, we obtain the finite-volume form for cell $ijk$,

$$\frac{\partial}{\partial t}\boldsymbol{q}_{ijk}+[\delta_I(\boldsymbol{H}\cdot\boldsymbol{S}_I)+\delta_J(\boldsymbol{H}\cdot\boldsymbol{S}_J)+\delta_K(\boldsymbol{H}\cdot\boldsymbol{S}_K)]_{ijk}=\Upsilon(\boldsymbol{q})\approx O(\Delta x^3), \tag{2}$$

where $\delta_I(\boldsymbol{H}\cdot\boldsymbol{S}_I)\approx(\boldsymbol{H}\cdot\boldsymbol{S}_I)_{i+\frac{1}{2}}-(\boldsymbol{H}\cdot\boldsymbol{S}_I)_{i-\frac{1}{2}}$ is the centred-difference operator. A more detailed description of the method is given in Rizzi & Eriksson (1984). With the appropriate boundary conditions, and representing all spatial differences by **FD**, we integrate this last equation with the two-level three-stage scheme

$$\begin{aligned}
\boldsymbol{q}_0 &:= \boldsymbol{q}^n,\\
\boldsymbol{q}' &:= \boldsymbol{q}_0+\Delta t\,\mathbf{FD}(\boldsymbol{q}_0),\\
\boldsymbol{q}'' &:= \boldsymbol{q}_0+\Delta t[\tfrac{1}{2}\mathbf{FD}(\boldsymbol{q}_0)+\tfrac{1}{2}\mathbf{FD}(\boldsymbol{q}')],\\
\boldsymbol{q}^{n+1} &:= \boldsymbol{q}_0+\Delta t[\tfrac{1}{2}\mathbf{FD}(\boldsymbol{q}_0)+\tfrac{1}{2}\mathbf{FD}(\boldsymbol{q}'')],
\end{aligned}$$

that steps the solution forward in time. Because a local time-step $\Delta t$ is used, true time accuracy is not obtained in the global sense†. But when a steady state exists, the procedure reaches it, and when one does not exist, the pseudo-time iterations do not converge. The method has been under development for more than ten years (see e.g. Rizzi & Bailey 1976; Rizzi 1982). It is well-tested, and in an extensive series of comparisons with other methods it has proven to be accurate and reliable (Smith 1985).

## 3. Features of computed Euler solutions

Some features commonly observed in numerical solutions to the Euler equations are currently under debate. Foremost among them, perhaps, is the creation of vorticity in the absence of a Kutta condition. Rizzi & Eriksson (1984) discussed this issue in regard to their solution for transonic flow past a quadrilateral wing with low sweep angle. Without invoking a Kutta condition, that solution displayed a vortex sheet being shed from the trailing edge of the wing, which is sharp. No rigorous proof exists, but it is generally thought that a vortex sheet being created at a discontinuous edge is a bona fide solution to the Euler equations. Hirschel & Fornasier (1984) argued that in a potential flow past such a wing, the upper- and lower-surface velocities are in substantial shear relative to each other over much of the chord. The shear disappears only just at the trailing edge, and if that edge is sharp, the numerical solutions to the Euler equations do not seem to obtain this shear cancellation. A vortex sheet forms instead. In the solution of Rizzi & Eriksson (1984), however, a vortex was also found at the rounded tip of the wing. It is currently believed that artificial viscosity is responsible for the formation of a vortex due to the shedding of a vortex sheet from a smooth edge.

Apart from the question of the creation of vorticity, a further issue is whether it is at all feasible to expect some degree of accuracy in the vortical structures of a mesh-based numerical solution. A close look at two alternative computational models

† Because the local time-step varies directly with the size of the individual cell, one can argue that in a smooth mesh the calculation is time-accurate locally.

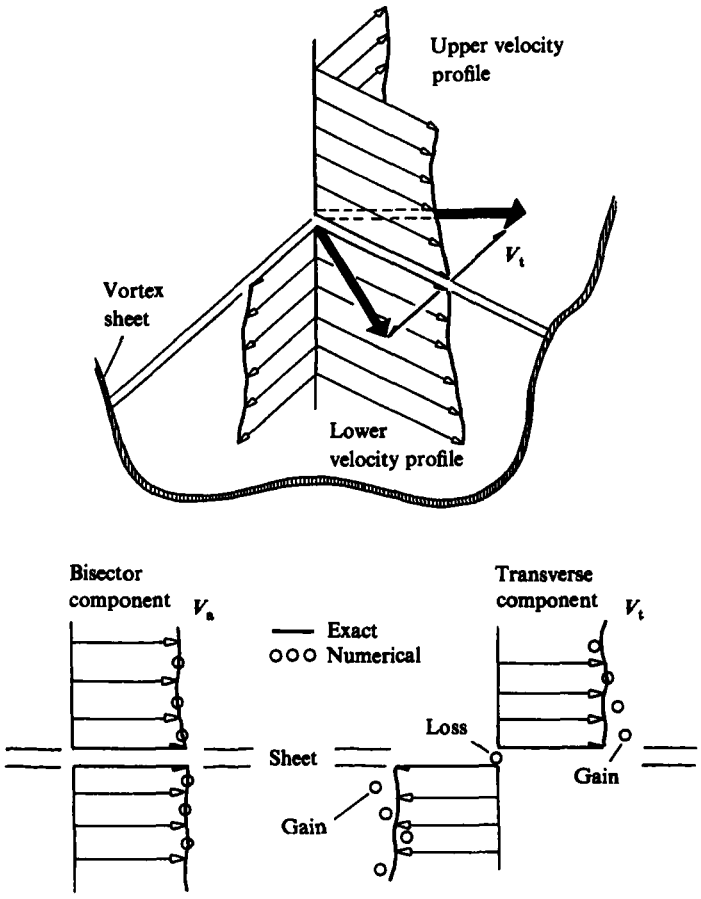


FIGURE 1. A vortex sheet has a discontinuity in velocity vector. Any numerical solution that supports the jump in the transverse component may show either a loss or gain in total pressure.

for inviscid incompressible vortex flow provides some insight. Hoeijmakers & Vaatstra (1983) have devised a method based upon a panel technique that inserts a vortex sheet into the solution as a discontinuity and adjusts it to be force-free in the surrounding potential field, usually termed vortex-sheet tracking. The strong point of this approach is the complete absence of diffusion of the sheet, while its limitation is that the overall starting location and topology of the sheet must be specified beforehand. An alternative is to solve the incompressible Euler equations numerically on a grid. The vortex sheet, smeared out over a number of mesh cells, is then obtained automatically as part of the numerical solution, usually termed vortex-sheet capturing (Rizzi & Eriksson 1985). Its weakness is that all the flow features must be supported by the mesh, and this implies a certain amount of dissipation that varies with the spacing of the mesh. Thus a vortex sheet diffuses over a number of cells. On the other hand, the strong point of this approach is that no information about the topology of the sheet needs to be specified prior to the solution. The smeared sheet can meander exactly as it likes, provided there are sufficient grid points to inhibit its diffusion and to maintain its general structure. A recent comparison of results from these two methods for incompressible flow past a conical

delta wing of finite length shows remarkable agreement in the position and strength of the vortical features (Hoeijmakers & Rizzi 1984). It demonstrates that even with a mesh of less than 80000 cells the diffusion has not brought about any substantial deterioration in the overall accuracy of the results compared to the diffusion-free solution. This finding strengthens our overall confidence in representing vortical-flow features upon a mesh.

The comparison of the results from the two methods brought out one striking fact – substantial losses in total pressure are encountered in the Euler solution, whereas total pressure is constant in the potential solution. Despite the losses, the two results agree rather well on the surface of the wing. Originally it was thought that the losses are strictly a function of the artificial viscosity in the solution, but Powell *et al.* (1985) have pointed out that it is, rather, a consequence of capturing the vortex sheet. The velocity across the sheet is sheared. In a coordinate system aligned with the bisector of the two velocities at the edges of the sheet, the bisector or axial component $v_a$ is constant across the sheet, but the transverse component jumps from positive to negative $v_t$ (figure 1). Somewhere within the sheet this component passes through zero and there the total pressure in isoenergetic compressible flow,

$$p_{t_{\min}} = p\left\{1+\frac{v_a^2}{2h_0-v_a^2}\right\}^{\gamma/\gamma-1},$$

reaches a minimum because $h_0$ is a global constant and the static pressure $p$ is constant across the sheet. Hence the loss in total pressure follows from the widening of the sheet, a consequence of the capturing of the weak solution which must be supported over several mesh cells. Because the axial component $v_a$ is continuous across the sheet, we assume that the numerical method represents it accurately. But the method is likely to produce over- and undershoots in the approximation of the jump in $v_t$ that result directly in gain or loss of total pressure. In a sense one can say that total-pressure loss is an effect of artificial viscosity, which is what gives the smooth profile across the sheet, but it is important to realize that the artificial viscosity does not determine the magnitude of the loss. The magnitude is set by the value of $|v_t|$, which is determined by the overall velocity field as it approaches the shedding edge. The structure within the captured sheet is, of course, not physical, being a direct consequence of the artificial viscosity model.

## 4. Mesh convergence and unstable modes

The flow model defined by (1) and (2) that we are using is second-order accurate, and strongly dissipates phenomena whose wavelength is of the order of the mesh spacing. One of the best means to judge the accuracy of a given numerical solution is to repeat the calculation with the mesh refined by halving the spacing in each of the spatial dimensions. The truncation error of the discrete scheme falls off quadratically, and the strength of the artificial viscosity in the regions of smooth flow is diminished even more rapidly, by $(\Delta x)^3$. Across discontinuities and sharp gradients of the flow the artificial viscosity is only linear in $\Delta x$, however, owing to the nonlinearly switched second-difference term of the model. One tries to compute a sequence of calculations with meshes progressively refined in this manner. When the sequence of solutions converges, one is confident that the truncation error and artificial viscosity have been reduced to an insignificant level, and that the solution is an accurate one.

If the true solution is laminar and contains only modes that are large in scale with

respect to the mesh size, then we can expect the sequence of refined-mesh approximations to converge to it. But if small-scale modes are excited, for example by a flow instability, the sequence will not converge. Reducing the mesh size increases the number of unknowns and increases the degrees of freedom of the solution. The smaller we make the mesh spacing by adding more grid points, the finer the scale-length of the phenomena that we can resolve without them being obliterated by the dissipation. In this way the numerical method acts as a low-pass filter on the features we observe, where the cutoff wavelength is set by the fineness of the mesh. This fact can be used to detect the presence of unstable modes. The usual mesh dimensions, giving say about 80000 cells, can support only the large-scale features, which we presume are stable. When we use a much finer mesh, smaller-scale features, if they are generated, are then represented in the numerical solution. The stability analysis by Moore & Griffith-Jones (1974) and Moore (1973) suggests that short-wave modes are the most unstable in the flows that we are discussing. By comparing the solution obtained with the usual mesh to the one obtained with the finer mesh and observing the differences between them, one can detect the presence of fine-scale structure and its influence on the overall flow. We hypothesize that, given a sufficient number of grid points to resolve the shed shear layer and limit its diffusion, the numerical solution of the Euler equations does provide useful information about the dynamics of the free shear layer around delta wings. In particular if the resolution is sharp enough, one may determine whether the vortical structures in the flow are unstable.

If this line of attack on the problem is to succeed, we must be able to refine the mesh sufficiently that the resolved spectrum reaches far enough into the small scales to capture the suspected unstable modes. If it does not, we shall never see the instability. The recent construction of supercomputers with many millions of words of real memory now allows the use of more dense meshes than was possible before. Of course there will always be those modes that are smaller than the resolution of our mesh, no matter how big our computer is, and we can say nothing about these modes. All we can do is construct several meshes of varying mesh fineness, and then compare the solutions computed upon them in order to establish the trend as the resolution increases.

## 5. The aim of the numerical experiment

We intend to test our hypothesis and search for unstable modes in the vortex dynamics around delta wings. The numerical experiment comprises two different vortex flows at transonic speed. The first case, a flat thin wing of pure delta form at a 10° angle of attack, is the classical sharp-leading-edge-vortex problem. The flow is very nearly conical and is subjected to a minimum of three-dimensional disturbances. In sharp contrast to this, the second wing form is chosen to be a twisted cranked delta wing with a cropped tip and a smooth leading edge, also at transonic speed and an 8° angle of attack. Owing to this geometry the flow is very non-conical and the vortex structures are expected to be highly three-dimensional. Progressively refined mesh solutions are carried out for both cases, with the intention of contrasting one case against the other in order to highlight the similarities as well as the differences. The discussion focuses on the controversial issues surrounding numerical Euler solutions: the creation of vorticity, the diffusion of vortical features upon the mesh, the loss of total pressure, and the stability of the vortex dynamics. We shall draw some conclusions about these issues from the two flows by looking at the

computed isobars, contours of total pressure, magnitude of vorticity, and some integrated particle paths.

The two cases are at transonic speed where there is a paucity of measured data because flow visualization is difficult to carry out in this regime in a wind tunnel. In a sense, then, the computations are exploratory in nature, with the aim of reaching at least a preliminary understanding of the dynamics of the vortex features that are involved. By these simulations, using even the highest numerical resolution possible, we cannot, however, hope to answer all the outstanding questions surrounding these issues. Our goal is more in the spirit of tracing a broad outline of the phenomena involved, along with offering some elementary explanations for their presence, as a means to establish a suitable phenomenological model. This may help to guide the way to a better understanding of the issues and a more fruitful analysis in the future.

## 6. Computed results for the pure delta wing

Transonic flow, $M_\infty = 0.7$, is the first case, computed around a flat 70° swept delta wing of zero thickness and incidence $\alpha = 10°$. The leading edge is sharp and the wing is pure in the sense that it is entirely conical, with the tip not cropped. It is the wing on which Hoeijmakers & Rizzi (1984) carried out their comparison for incompressible flow, and further results were discussed by Rizzi & Eriksson (1985). It is also the wing for which Murman, Rizzi & Powell (1985) obtained very good agreement at supersonic speeds between two-dimensional conical and fully three-dimensional computations, both using very high-resolution meshes.

Here at transonic speed we use the same 0–0 mesh topology as those two previous investigations. Figure 2 presents chord and span sections, as well as a three-dimensional projection of the mesh. The mesh is drawn for dimensions $80 \times 24 \times 40$ cells, but we calculate here with $192 \times 56 \times 96$ for just over one million cells. The outer extremity of the mesh is a hemisphere (assuming centreline symmetry) with a radius of about 3 root chords $c_r$ of the wing. The computation begins with the free-stream values as initial conditions on the so-called coarse grid of dimensions $48 \times 14 \times 24$ obtained by using only every fourth point in the original mesh. One thousand iterations are carried out, the results are interpolated to the medium mesh $96 \times 28 \times 48$ where another 1000 iterations are performed, and this successive global mesh refinement is repeated once again to reach the fine mesh of $192 \times 56 \times 96$ cells. Figure 3 presents the evolution of the lift coefficient $C_L$ and the decay in the density residual, the $L_2$ norm of the change in density from one iteration to the next. We see that the decay rate $d$ is greatest in the coarse mesh and least in the fine, reflecting its character, $d \approx 1 - O(\Delta x)$. As the mesh grows finer, transient waves require more time iterations to pass through a given region of space. Still, one can see that a steady state is reached after 1000 iterations on the fine mesh. The residual is reduced by three orders of magnitude and the lift is steady at $C_L = 0.448$.

Next we examine the flow field for its content and quality of vortical features, and we also want to determine if the fine solution is converged in the sense of mesh spacing. Side-by-side surveys of the medium-mesh and fine-mesh flow fields are suitable for this purpose. Figure 4 shows the fluid-particle paths that are integrated from the steady velocity field by selecting a number of positions distributed along a line near the leading edge as seed points and then tracing their path downstream. Alternatively, a line $x =$ constant along the span can also be chosen. In either case the differences between the medium and fine streamlines are very small. In both flow

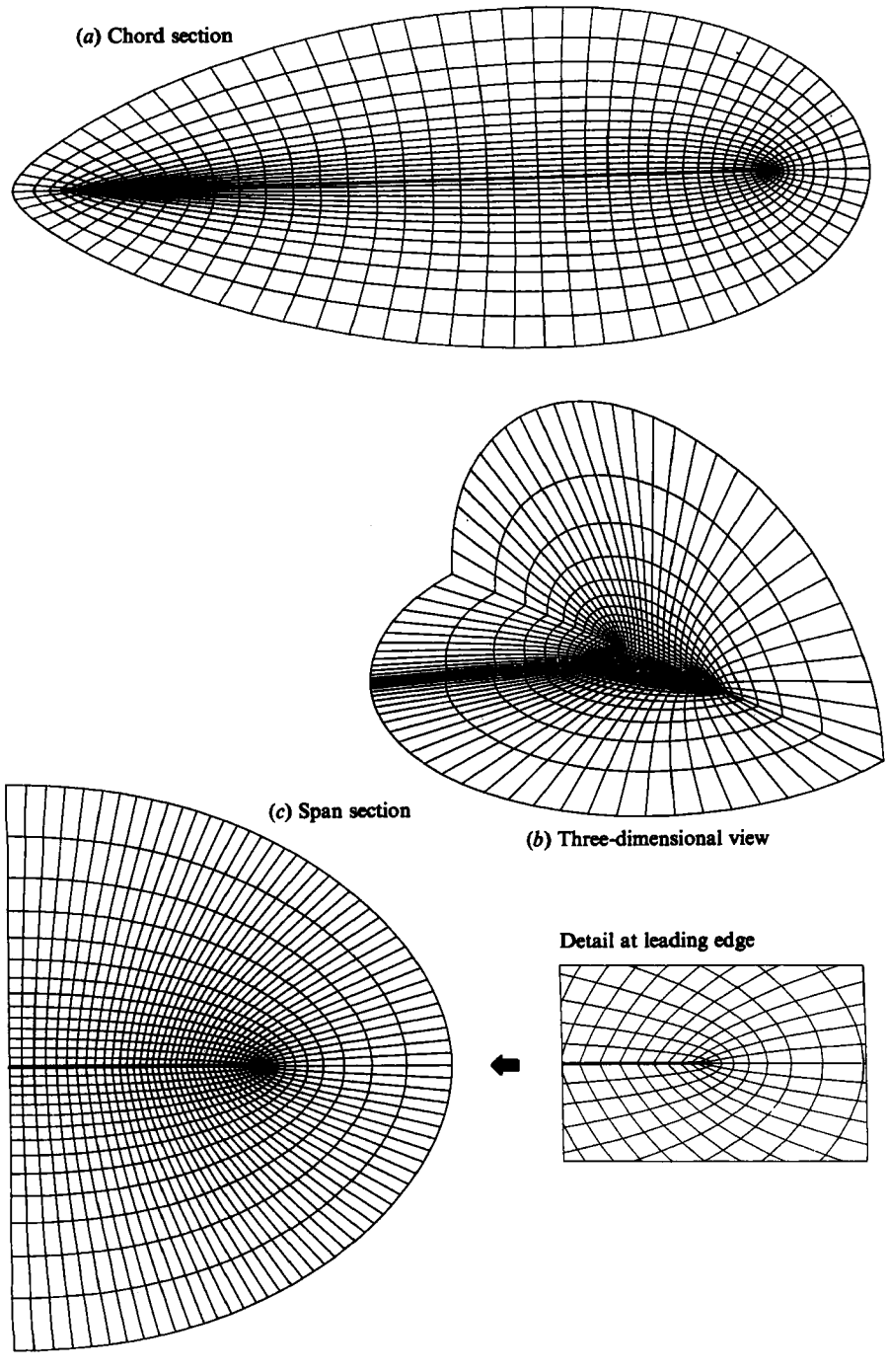


FIGURE 2. Grid generated around a slender delta-shaped wing has an 0–0 topology that concentrates points around the edges.

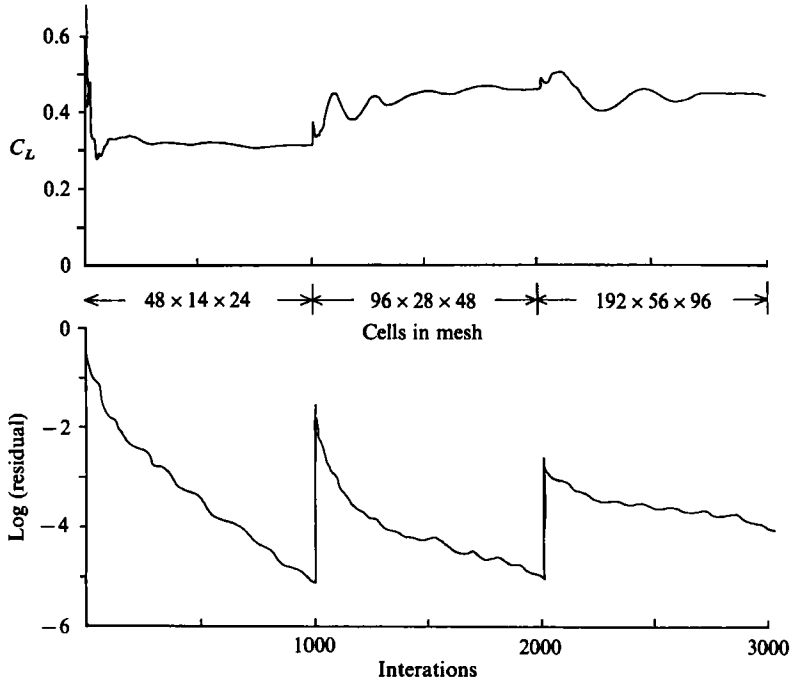


FIGURE 3. Evolution of lift coefficient $C_L$ and decay of $L_2$ residual over three-grid sequence of solutions: pure delta, $M_\infty = 0.7$, $\alpha = 10°$.

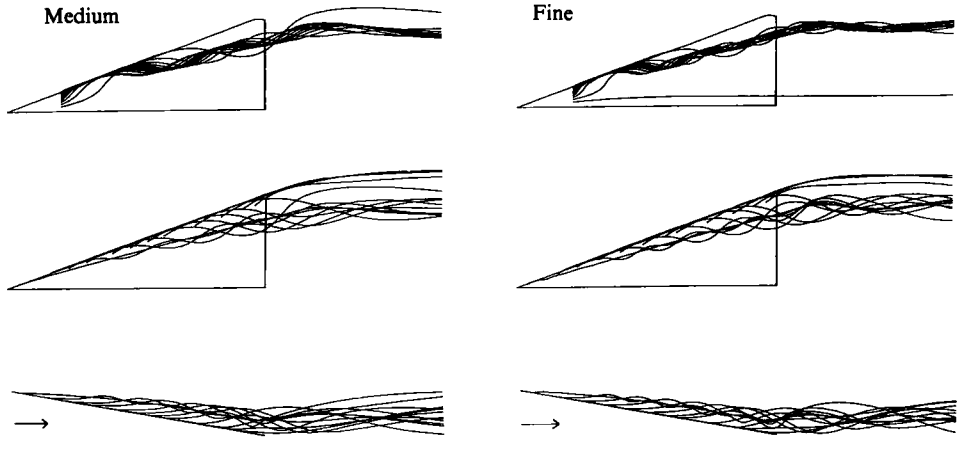


FIGURE 4. Comparison of integrated particle paths from medium- and fine-mesh solutions.

fields, separation begins at the apex and continues all along the leading edge, and a vortex evolves.

There is no doubt that the numerical method is selecting the solution with the shed vortex sheet. It would be futile to think that one could obtain the attached potential solution for this case because that would require the cancellation of the shear between the upper and lower surface all along the geometrical singular line of the leading edge. The method prefers instead to allow the shear to separate there in a vortex sheet, which is an allowable solution of the difference equations. The sharp

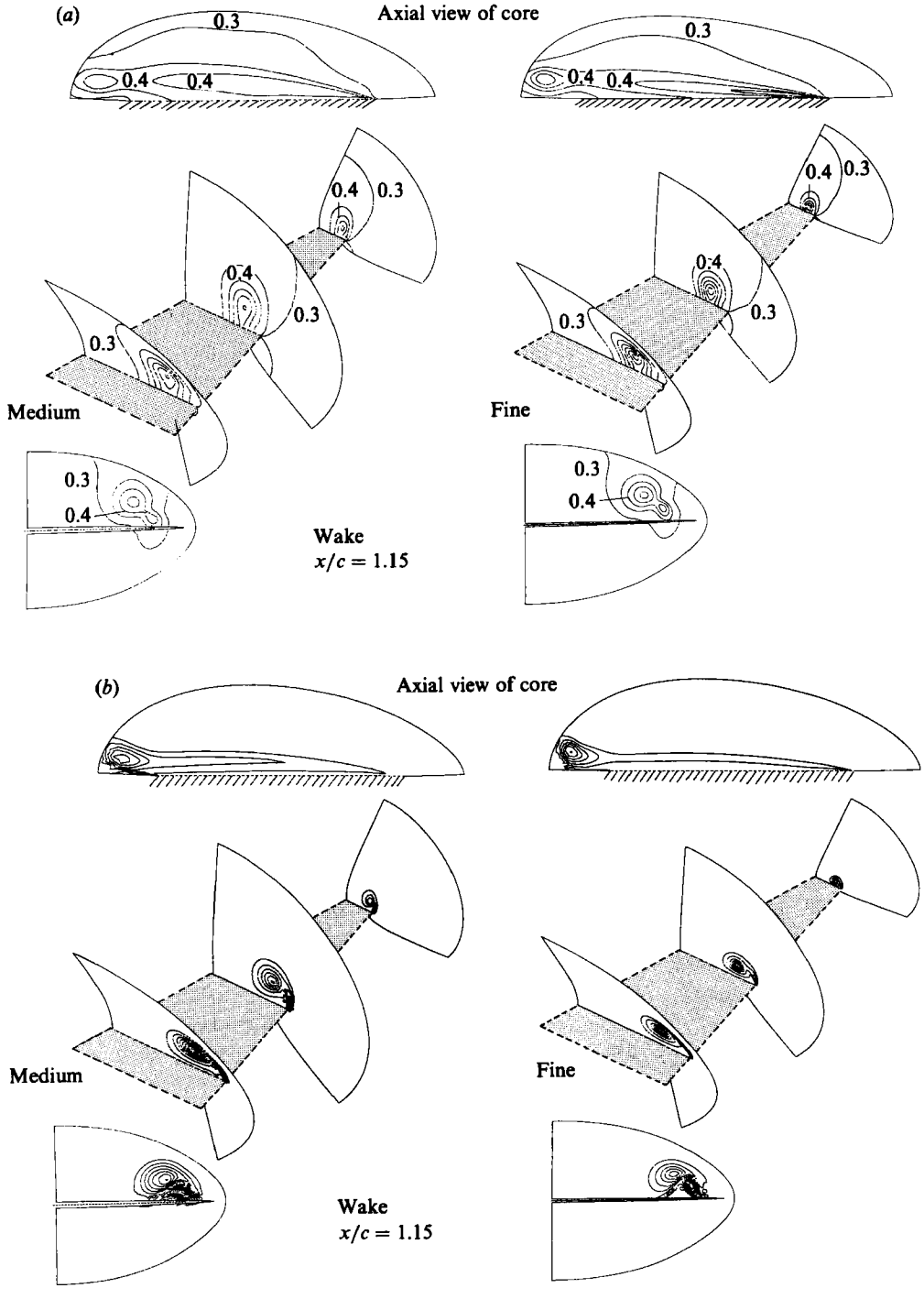


FIGURE 5(*a*, *b*). For caption see p. 175.

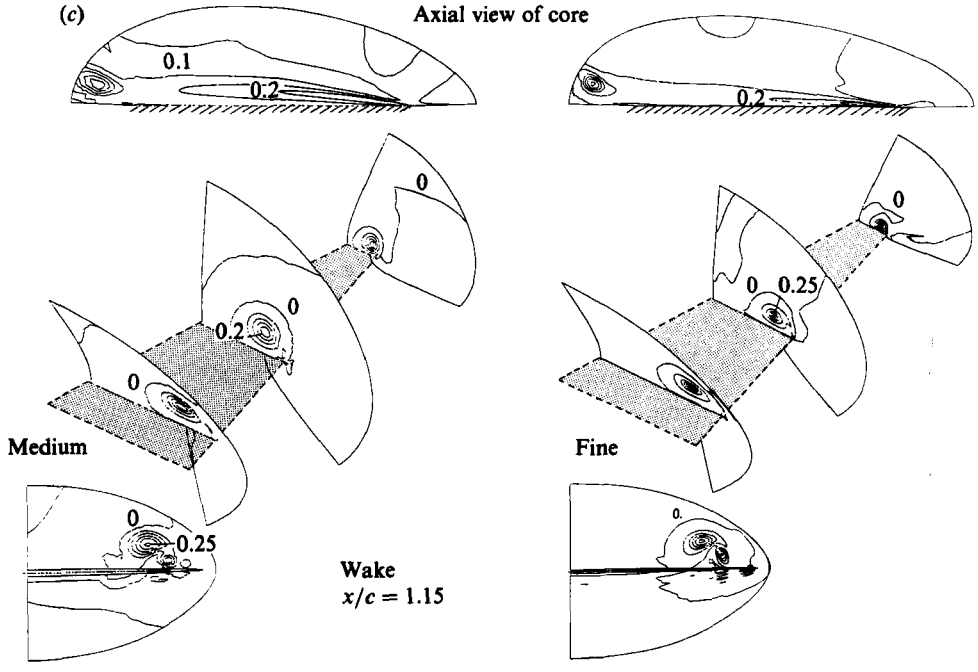


FIGURE 5(*c*). For caption see facing page.

leading edge in this case plays the corresponding role to the trailing edge of the high-aspect-ratio wing in Rizzi & Eriksson (1984).

The flow fields of the medium and fine solutions are very nearly conical and the vortex cores lie practically in a straight line, except beyond the trailing edge where the vortex is turned inboard and upward in order to return to the free-stream direction further back. It is the increasing pressure gradient, from a low value in the vortex core over the wing to the higher free-stream value beyond the trailing edge, that brings about this effect. At higher angle of attack this three-dimensional disturbance can be sufficiently large to produce a spiralling of the core and, eventually, vortex breakdown (Hall 1972; Leibovich 1978).

The isocontours of the medium and fine solutions in figure 5 confirm the conclusion that the flow is smooth and nearly conical and that the differences between the two of them are only small. The isobars (lines of constant ratio of local static to free-stream total pressure, $1-p/p_{t_\infty}$) in figure 5(*a*) indicate a low-pressure region in the core that changes little from the medium to the fine solution. The detail in the wake structure is sharper in the fine solution, and the axial view of the core might suggest that the fine core lies a little closer to the wing than the medium core. The feature just past the trailing edge in this view is a function of the curved mesh surface, in which the contours are drawn, cutting across the vortex. It should not be mistaken for a spiralling motion. The survey of vorticity magnitude $|\boldsymbol{\Omega}|$ in figure 5(*b*) reveals a sharper resolution of the vortex sheet separating from the leading edge, and the interaction of the leading-edge and trailing-edge vortices in the wake. Aside from the crisper resolution of the sheet, the agreement in the overall features here implies that the vortex dynamics can be represented in numerical solutions upon a mesh to a good degree of accuracy. Both solutions indicate that the vorticity in the sheet falls off rapidly over a short distance from the leading edge. This would suggest that even

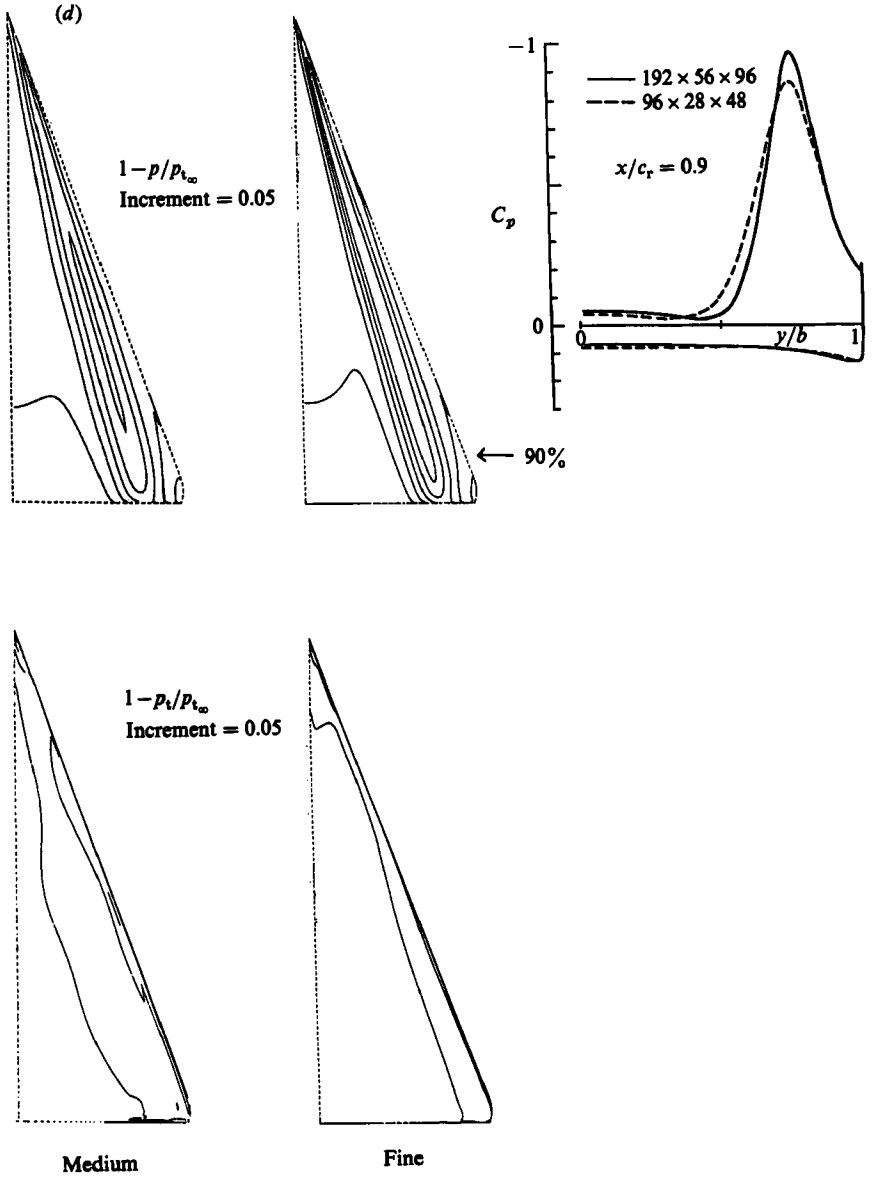


FIGURE 5. Isograms comparing the medium-(96 × 28 × 48) mesh and fine-(192 × 56 × 96) mesh solutions drawn in a number of mesh surfaces around the pure delta wing: $M_\infty = 0.7$, $\alpha = 10°$, increment = 0.05. (*a*) Pressure $1-p/p_{t_\infty}$; (*b*) vorticity magnitude $|\boldsymbol{\Omega}|$; (*c*) total pressure loss $1-p_t/p_{t_\infty}$; (*d*) upper-surface contours.

before completing the first turn of its spiral the strength of the sheet is rather small. It might not be very important, therefore, to resolve the coils of the spiral distinctly. The concentric rings of increasing vorticity magnitude indicate the vortex core, where swirl velocity is diminished and converted into axial velocity. One can see this effect in the pathlines in figure 4. This is a dissipative process, as evidenced by the loss in total pressure (figure 5*c*), and presumably the result of either truncation error or numerical viscosity, or both. It is dependent on mesh size; the core shrinks as the mesh is refined, but it produces the realistic effect of zero swirl at the centre of the

core. Apparently the location of the core centre does not change significantly with mesh size (see also figure 4). The largest differences between the medium and fine solutions are seen in the contours of total pressure loss $(1-p_t/p_{t_\infty})$ in figure 5(*c*). The differences appear not in the level of the loss, which is about the same (20%) in the two solutions, but in the location. In the fine-mesh solution the corresponding contours are wound tighter in the vortex core. This observation is consistent with our discussion about the vorticity contours, and with the explanation of total-pressure loss given by Powell *et al.* (1985). The maximum loss is set by the shear at the leading edge, which seems to be reasonably well resolved in both the medium and the fine solutions. This shear determines the swirl that is swept up into the core. How it then diffuses in the core is a function of the mesh size there. One can surmise that on the fine mesh more of the sheet is distinctly resolved as it spirals up, and the core, where the swirl velocity goes to zero, is correspondingly smaller. Even in the fine mesh, however, it seems doubtful that more than one turn of the spiral is represented distinctly. Mesh-computed solutions must produce diffuse vortex cores within which the details have to be looked upon as somewhat artificial. Qualitatively, however, the concentric rings of total pressure in figure 5(*c*) are similar to those measured in experiments. Furthermore, we presume that the fine details of the core do not substantially alter the broad dynamics of the vortex structures.

The differences in the two solutions on the upper surface of the wing (figure 5*d*) are also small. The lowest-pressure contour in the medium solution falls off before the 90% span station. The low-pressure trough also is somewhat broader, but it is centred on the one in the fine solution. Also total-pressure loss has diffused onto the upper surface less in the fine solution than in the medium one. These are precisely the effects of mesh refinement reported by Rizzi (1987*a*, 1985*a*) for this wing in incompressible flow and for the Dillner wing in transonic flow, respectively.

In summary we conclude that for this case of low helicity (defined as the angle between the local velocity and vorticity vectors) and small three-dimensional departure from conical flow we have very nearly reached mesh convergence with our numerical solutions. The vortex flow here is laminar, and composed only of large-scale modes.

## 7. Vortex-sheet dynamics under large disturbance

The vortex core of the previous case is nearly straight. Betchov's (1965) analysis of an incompressible vortex filament shows that if it is forced to bend it begins to spiral, and its dynamics may become chaotic. The motivation of our next case is to observe the dynamics produced in a mesh-based solution of the Euler equations when the basic vortex structures are curved. In addition to being of practical interest, a cranked delta wing is a geometry suitable for producing this effect because it is non-conical. Our goal is to carry out an exploratory set of progressively refined computations for the flow field around such a cranked delta, in order to observe the vortex dynamics predicted by the mesh-based Euler solution and to make further remarks about the plausibility of the numerical model for the case when the vortex undergoes a large disturbance.

Since cranked delta wings have been studied mostly at low speeds, our discussion of the likely dynamics should begin for the case of incompressible flow (Thompson 1985). At some angle of attack a vortex sheet is shed from the leading edge. Figure 6 outlines three possible scenarios for the dynamics of that sheet. The wing is sketched with a side edge at the tip, which gives rise to a tip vortex, but our discussion is

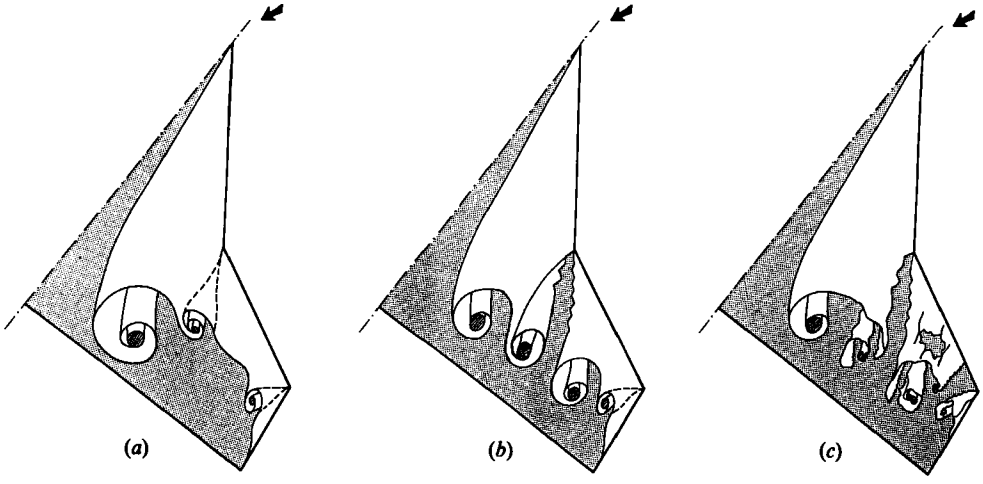


FIGURE 6. Three scenarios for the dynamics of the shed sheet: (*a*) intact sheet with double-branched spiral, (*b*) sheet tears but is stable, (*c*) sheet tears and is unstable.

concerned mainly with what happens at the crank in the leading edge. The model Hoeijmakers, Vaatstra & Verhaagen (1983) use to study this configuration assumes that at the crank the sheet remains intact but the change in sweep angle sets up a disturbance that causes the sheet to coil up into a double-branched spiral (figure 6*a*). In the scenario of Brennenstuhl & Hummel (1982), based on wind-tunnel observations, the sheet tears at the crank (figure 6*b*) and leaves a section inboard whose two free edges spiral up to form an inboard vortex which is not fed beyond the crank. The section outboard, if a sheet is shed at all, also rolls up into the outboard vortex. In both scenarios two distinct vortices of like sign are created and rotate about one another. The flow structure of these models is taken to be stable and composed only of large-scale motions. As the angle of attack increases, the corotating vortices have been observed to merge before reaching the trailing edge (Thompson 1985). At still higher angles of attack the occurrence of vortex breakdown has been reported (Brennenstuhl & Hummel 1982). This then leads to the third scenario (figure 6*c*) which suggests that the tearing process may bring about an instability in the sheet, which may well be a precursor to complete breakdown. Two vortices still form here, but the sheet shreds at the crank and, together with the two cores, they all disintegrate into a less-ordered, but standing-wave, pattern of vortical structures. Helicity in this case would be high because the vorticity and velocity fields are disordered and are no longer closely aligned. The details of this scenario are still matters of conjecture, for there is not yet any clear-cut experimental evidence to provide more certainty.

## 8. Computed results for the cranked delta

The delta wing selected for the experiment has a forward leading edge sweep of 57° which is then 'cranked' to 45° somewhere past 60% span. It is made up of a symmetric 4% thick profile that is constant over the span. The leading edge is smooth. Twisting the wing up at the root and down at the tip (figure 7) does not allow the flow to be conical and enhances the spatial dimensionality of the vortex dynamics.

Since the wing is given a side edge, the 0–0 type mesh topology of Eriksson (1982)

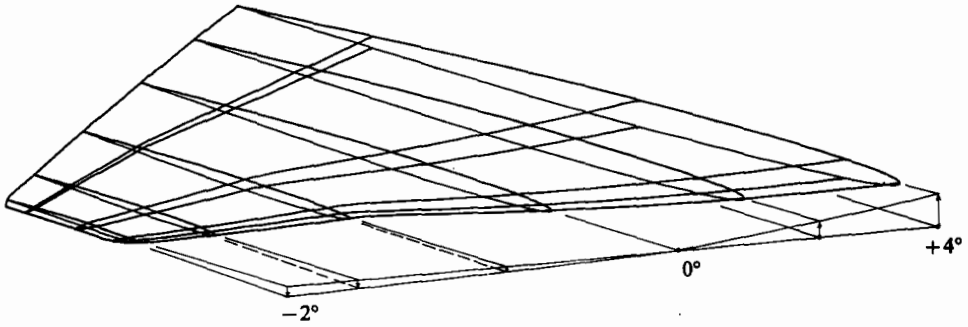


FIGURE 7. Cranked delta wing of constant symmetric profile and twist.

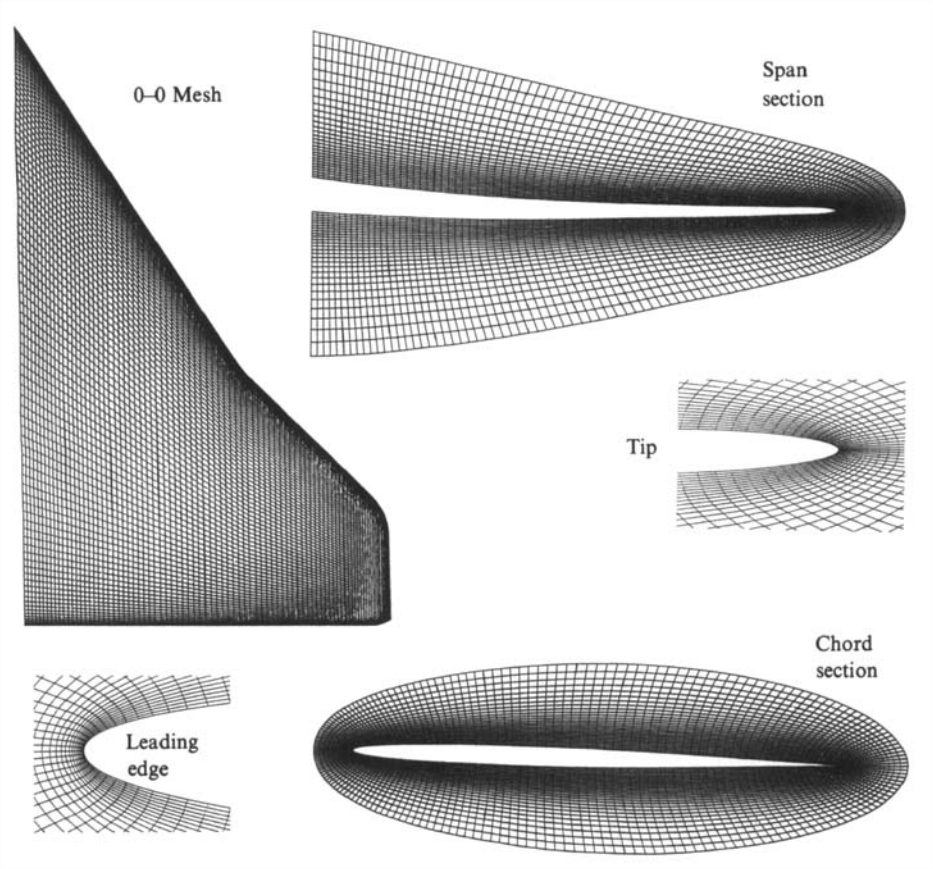


FIGURE 8. 0–0 type mesh with $192 \times 56 \times 96$ cells around cranked delta wing.

designed for trapezoidal planforms is suitable here. We have used this type of mesh before for a similar cranked delta wing (except that it is cambered) for cases at low angle of attack, when the flow remains attached around the leading edge. The computed Euler solutions agree very well with the results of a panel method, as well as with experimental measurements (Fornasier & Rizzi 1985). Comparisons like these give us confidence that the mesh is basically sound – its outer extremity is sufficiently far, and it is sufficiently smooth around the crank. At higher angles of attack, when the flow does separate at the leading edge and the panel method no longer applies, the overall lift and drag coefficients of the computed Euler solutions also agree well

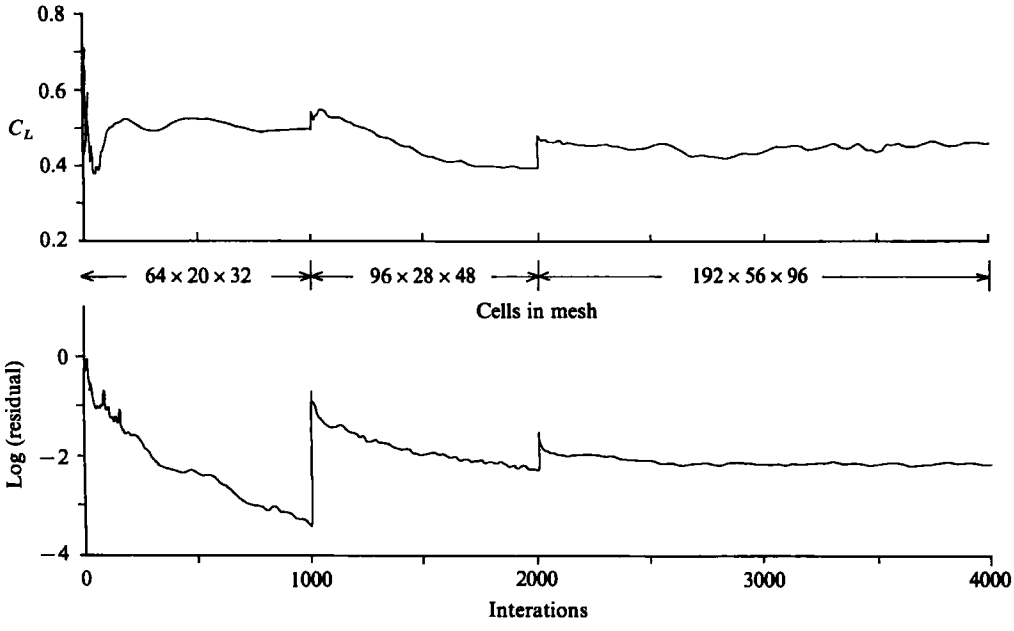


FIGURE 9. Evolution of lift coefficient $C_L$ and decay of $L_2$ residual over three-grid sequence of solutions: cranked delta, $M = 0.9$, $\alpha = 8°$.

with the measured values, but the comparison of surface pressures begin to show some discrepancies (Fornasier & Rizzi 1985; Rizzi & Purcell 1986*a*, *b*). An investigation with one level of mesh refinement failed to show mesh convergence. Instead, the refined-mesh solution with about 600000 cells indicates the presence of small-scale modes and the onset of non-smooth flow.

Here we want to further examine this observation under more carefully controlled conditions. The wing now is uncambered (figure 7), and the mesh-refinement sequence consists of three solutions with the last involving just over one million cells, the finest mesh that we can work with at this time. The flow conditions now are $M_\infty = 0.9$ $\alpha = 8°$ past the cranked-and-cropped delta wing with twist (figure 7). In the experiment we carry out the test for mesh convergence with three separate simulations, identical in every way except for the size of the grid, in order to compare the character of the flow represented on each of these grids and to judge if the sequence converges as it did for the pure delta wing. The fine mesh, identical in size with the one for the pure delta, has 192 cells around the chord of the wing, 96 cells across the span, and 56 from the wing surface outward to the far-field boundary, which is about 3 root chords away. Figure 8 presents the mesh in planform, chordwise, and spanwise sections. The medium mesh is produced from the fine one by eliminating every other cell wall in each direction, giving $96 \times 28 \times 48$ cells. For the coarse mesh every third cell wall in the fine mesh is retained, the two intervening ones are removed, and this leaves $64 \times 20 \times 32$ cells. Only the size of the cells differs in the three meshes; the outer boundaries are at the same location, and the relative distributions of cells are all identical.

Figure 9 reveals the evolution of lift and the decay of the $L_2$ norm of the density change over the course of the three-level mesh refinement. In the coarse mesh the residual is substantially reduced and a steady state is reached after 1000 iterations. The residual decay is much weaker in the medium mesh, and considerably less than

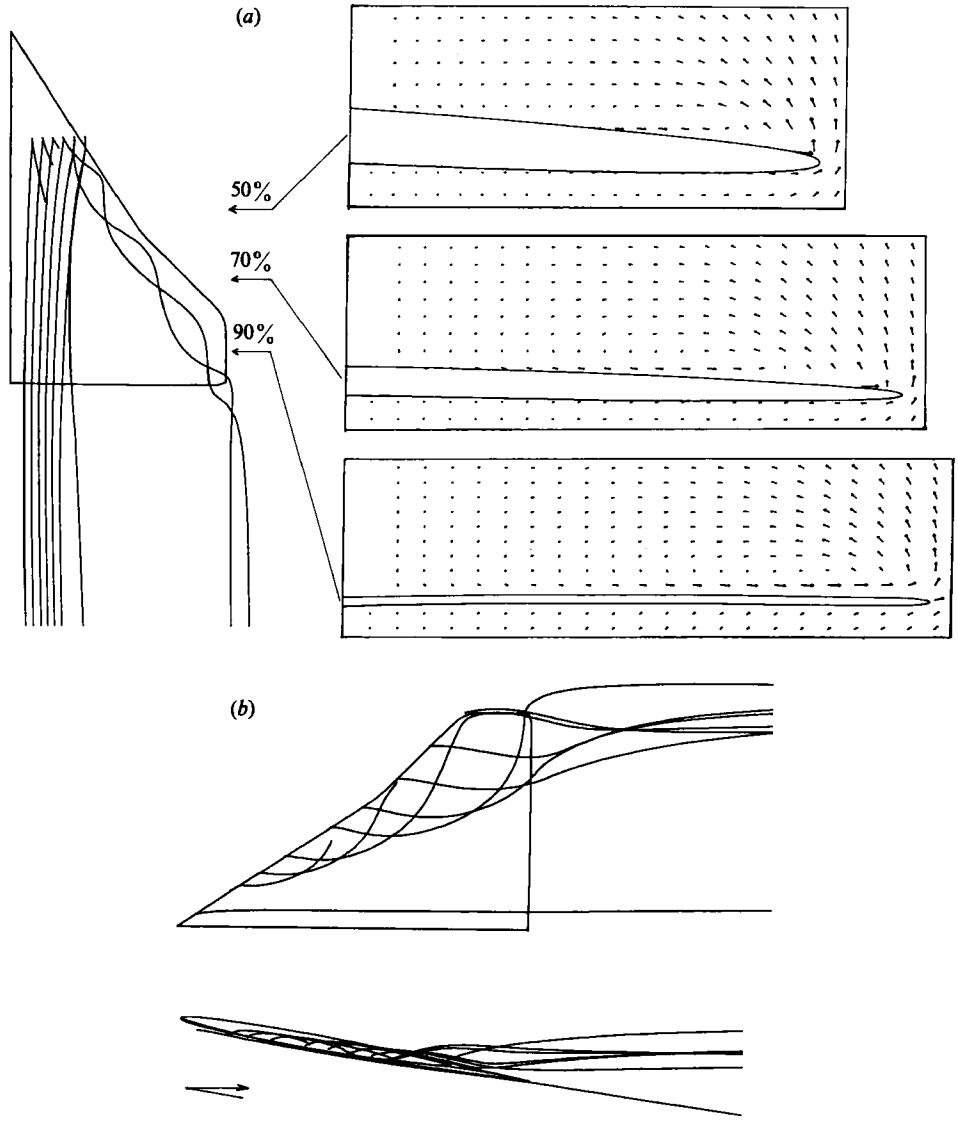


FIGURE 10. Integrated particle paths and $(v, w)$-velocity vectors from coarse solution, $64 \times 20 \times 32$ cells. (*a*) Particle seeding, $x$ = constant; (*b*) particle seeding along leading edge.

the medium-mesh evolution of the pure-delta case in figure 3. After a feeble initial diminishment following the interpolation from the medium result, the decay rate is virtually zero in the fine mesh even after 2000 iterations. This stands in marked contrast to the pure-delta case in figure 3, where a steady state was reached in 1000 iterations. Although most people would label this evolution as lacking convergence to the steady state, we prefer to call the solution after 2000 iterations in the fine mesh 'quasi-steady'. There are no growing components in the solution, the residual is more than two orders of magnitude below what it started out as in the coarse mesh, and the lift coefficient $C_{\mathrm{L}}$ shows only small-amplitude oscillations about a mean value. We believe, and we present observations to substantiate this point below, that this flow field is quasi-steady, not because of a malfunction of the numerical method, but owing

to the appearance of small-scale unstable modes of low energy content that on average do not alter the large-scale features of the flow. This matter of unstable modes in a numerical solution is a controversial one and needs much more clarification. To begin, we present our side of the debate.

### 8.1. *Coarse-mesh solution*

Since the coarse solution does reach a steady state, let us examine this flow field first. Figure 10 represents the streamlines integrated from this solution together with $(v, w)$-velocity component vectors drawn in the spanwise planes $x/c_r = 0.5$, 0.7 and 0.9, in order to observe better the details in the motion ahead of the crank, after the crank but ahead of the tip, and beyond the leading edge of the tip. These velocity vectors lie in a true plane, not a mesh surface, and they have been interpolated from the solution and equispaced in the plane so that the velocity in each of the mesh solutions may be compared at the identical location in space.

Figure 10(*a*) immediately demonstrates that a vortex does develop over the wing. Because of the smooth leading edge it starts not at the apex but about 20% $c_r$ downstream, where the streamlines show a very strong shearing. Twelve seed points are used, six very close to the upper surface and the other six just slightly above them. The integrated paths reveal that while some of these particles remain attached all the way to the trailing edge, others very nearby are swept outboard to the leading edge, separate, and roll-up into a single vortex. The velocity vectors confirm this pattern. It seems that in this coarse solution the shed vortex sheet remains contiguous. The vortex core does not follow the leading edge after the crank; instead it remains in a straight line but the sheet continues to be shed from the cranked leading edge. The crank produces a strong spanwise flow over the surface of the wing which then runs into the sheet from the tip and separates upward. The dramatic effect of the crank and tip, seen in the side view, figure 10(*b*), causes the vortex to lift upward away from the wing in the direction of the free stream. In the pure-delta case this phenomenon occurs only past the trailing edge. It is an indication that the cranked-delta flow field is highly non-conical.

The structures in the flow field are surveyed by contour plots of the flow properties in the three spanwise (true) planes, $x/c_r = 0.5$, 0.7, 0.9, and the upper wing surface. The plots are (*a*) static pressure (either $1-p/p_{t_\infty}$, normalized by the free stream total pressure, or the pressure coefficient $(p-p_\infty)/\frac{1}{2}\rho_\infty V_\infty^2$) to identify shock waves and expansion regions; (*b*) vorticity magnitude $|\boldsymbol{\Omega}|$ to bring out the vortical structures; and (*c*) total pressure coefficient $(1-p_t/p_{t_\infty})$ to show the shear layers and the shocks. By comparing these three sets of contours, one can differentiate the shear layers from the shocks. The contours in figure 11 confirm the picture given by the streamlines in figure 10. The pressure (figure 11*a*) on the upper surface has a ridge-like pattern, the typical footprint of the vortex. The isobars remain smooth and intact and follow the leading edge by bending slightly around the crank. This leads us to think that only one vortex core forms and that the shear layer is probably contiguous in this solution. It appears, however, that the crank in the leading edge intensifies and focuses the vorticity because the vorticity contours are stretched out by the protruding leading edge at the 70% plane (figure 11*b*). The vorticity contours in all three planes verify that a high-intensity vortical layer is shed from the leading edge, and the concentric pattern reaffirms a single-core vortex. The total-pressure contours (figure 11*c*) follow the pattern of vorticity as they should, and indicate a loss of 50% in the core. The contours in the 90% plane imply a welling up of the vortical layer near the leading edge. To judge by the ridge of the pressure trough and the build-up

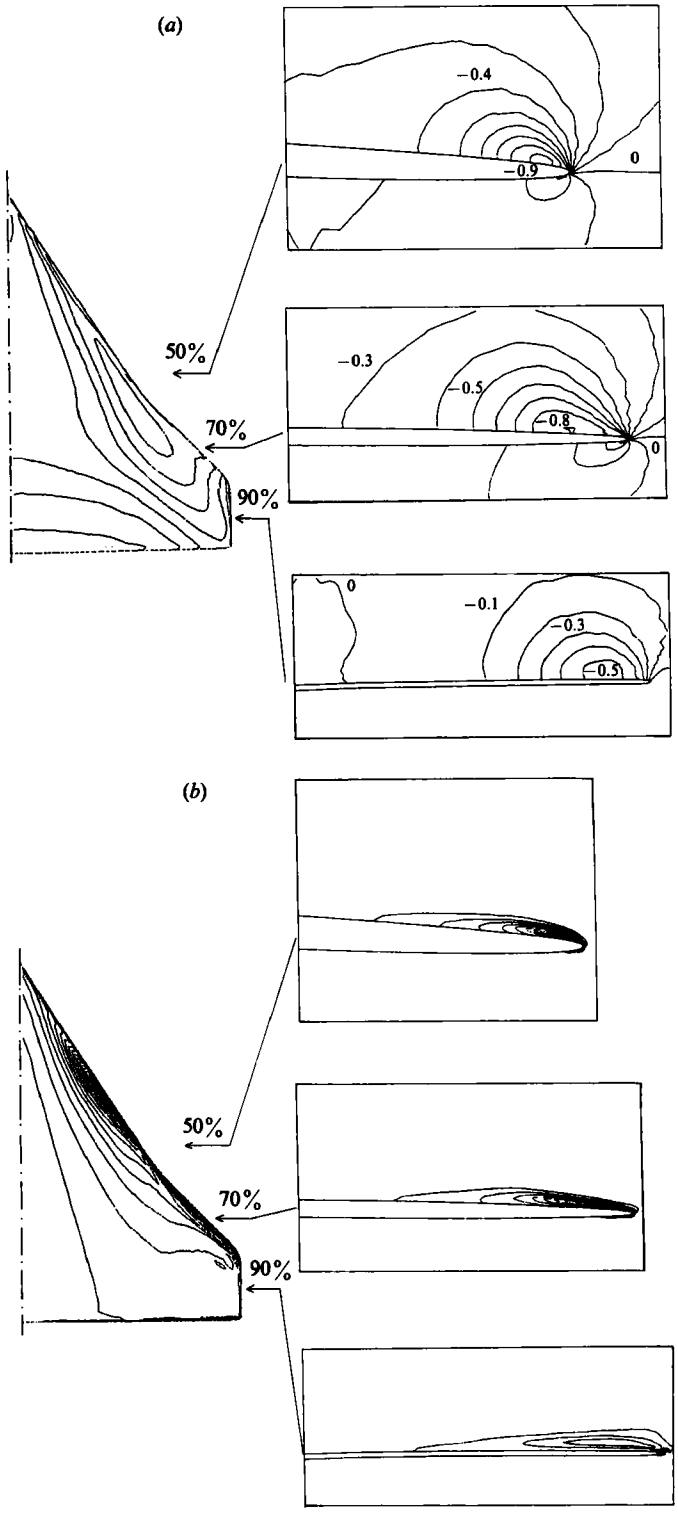


FIGURE 11 (*a*, *b*). For caption see facing page.

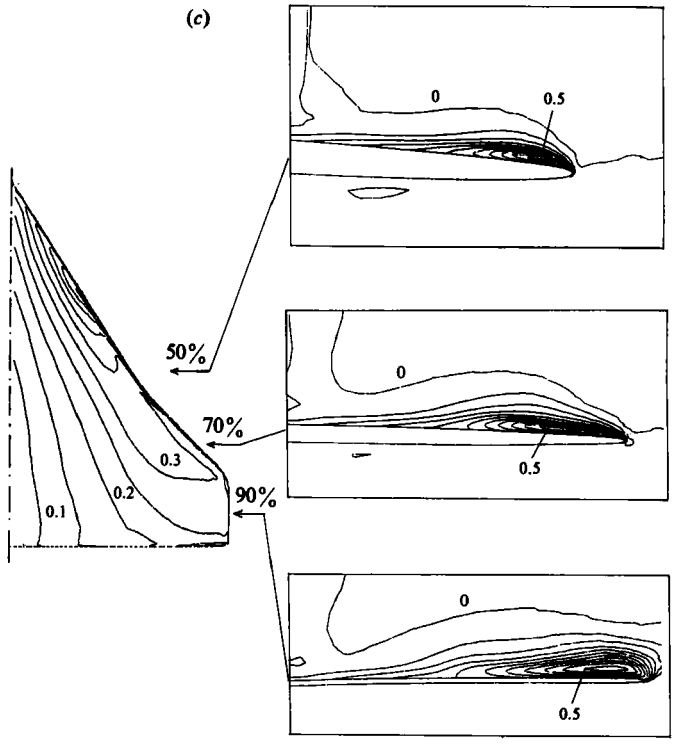


FIGURE 11. Isograms of the solution computed around the cranked delta using the coarse $64 \times 20 \times 32$ mesh, $M = 0.9$, $\alpha = 8°$. (*a*) $C_p$ isobars (increment = 0.1); (*b*) vorticity magnitude (increment 0.005); (*c*) total pressure, $1 - p_t/p_{t_\infty}$ (increment 0.05).

of vorticity along the leading edge, the vortex begins on the leading edge at about $x/c_r = 0.2$. Inboard of the vortical region the flow is attached (figure 10) and a gradual recompression takes place just ahead of the trailing edge (figure 11*a*). Figure 11 overall confirms the laminar quality of the shear layer shed from the leading edge and outlines the diffuse features that we might expect from this coarse-grid solution. One sees that it contains only long-wave components. The behaviour of the sheet, if it can be distinguished at all, seems closest to scenario 1 (see figure 6), although there is no evidence of a double-branched roll-up at the crank.

### 8.2. *Medium-mesh solution*

We now want to learn if the sequence of solutions under mesh refinement converges to a laminar result, as it did for the pure-delta case. When the mesh is refined $1\frac{1}{2}$ times in each of the three directions to the medium mesh of dimensions $96 \times 28 \times 48$, the streamlines that result are shown in figure 12. The vortex starts at about the same location on the leading edge as in the coarse solution, but now inboard of the crank the core is less diffuse and more tightly wound (figure 12*a*). At the crank an abrupt transition takes place and the pathlines in the vortical layer downstream become disordered. The layer wells up into a bulge ahead of the trailing edge (figure 12*b*), certainly with high helicity content. After losing 50 % of its total pressure, the flow has to slow down substantially to meet the rising pressure gradient. As discussed by Murman & Rizzi (1986) the loss of total pressure may be a significant event in the breakdown process.

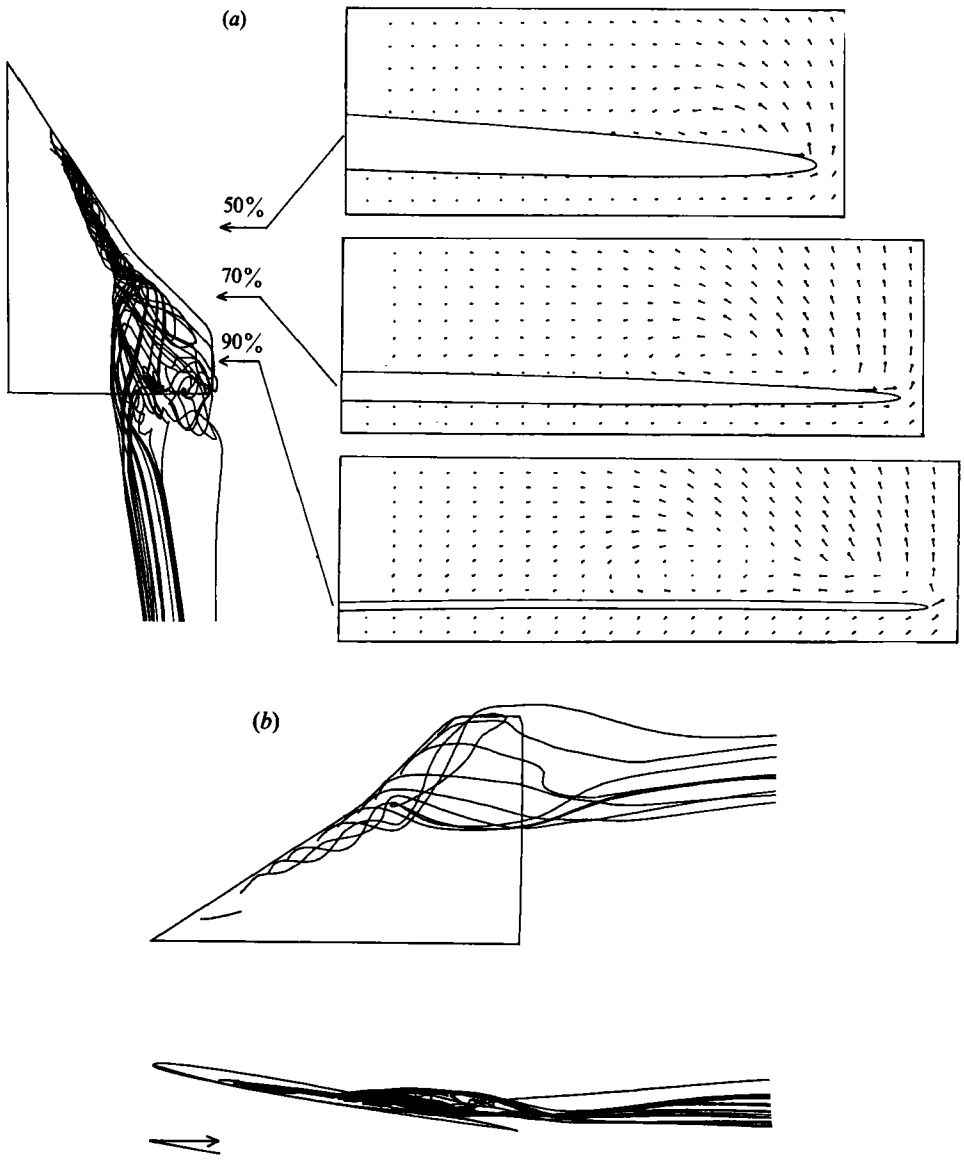


FIGURE 12. Integrated particle paths and $(v, w)$-velocity vectors from medium solution, $94 \times 28 \times 48$ cells. (*a*) Particle seeding near vortex start; (*b*) particle seeding inboard from leading edge.

Compared to the coarse solution, the elongated ridge-like contours of low pressure along the leading edge do not bend smoothly and continuously around the crank (figure 13*a*). Instead the innermost ones are terminated, and the others sprawl over the outer wing surface in a wavy manner. Outboard of the crank other contours begin to build up again at the leading edge, but without the usual ridge-like pattern. It seems that in these results the shear layer from inboard undergoes a disturbance at the crank, which partially depletes its well-organized structure, and that although weaker, this shear layer continues to be shed along the leading edge past the crank but does not roll-up in the usual spiral to form an outboard vortex. The vorticity contours (figure 13*b*) provide some clues for the interpretation. The build-up of

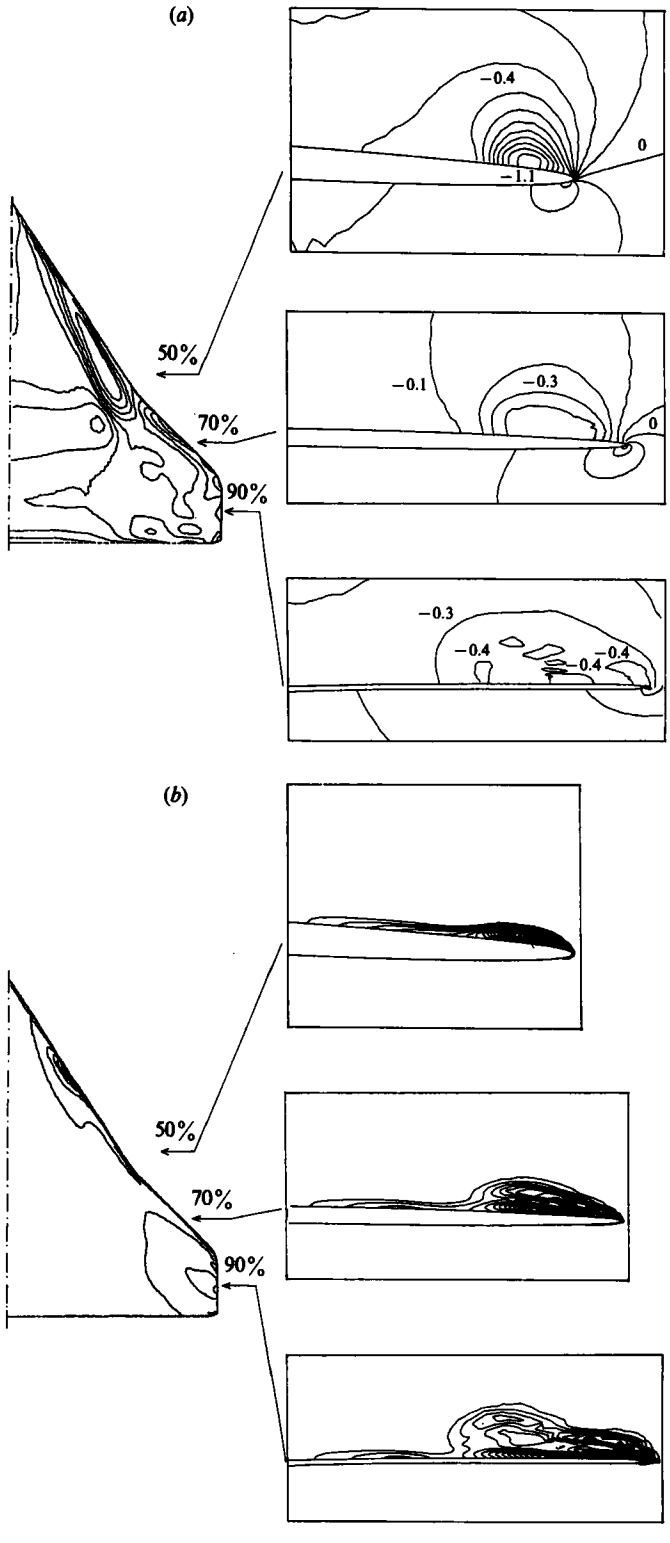


FIGURE 13(*a*, *b*). For caption see next page.

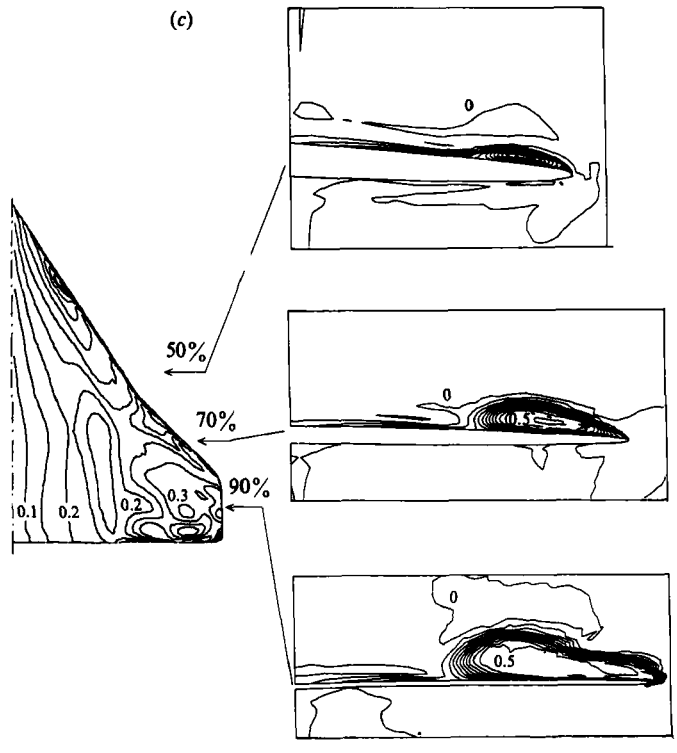


FIGURE 13. Isograms of the solution computed around the cranked delta using the medium $96\times28\times48$ mesh, $M=0.9$, $\alpha=8°$. (*a*) $C_p$ isobars (increment = 0.1); (*b*) vorticity magnitude (increment 0.005); (*c*) total pressure, $1-p_t/p_{t_\infty}$ (increment 0.05).

vorticity at about $x/c_r = 0.2$ on the leading edge signals the start of the inboard vortex, and its single core is evident in the 50 % plane (figure 13*b*). After the crank the pattern changes to that of two extrema of vorticity in the 70 % plane. This suggests that the crank may be setting off the double-branched spiral of scenario 2 (see figure 6), which then evolves into two distinct vortices. It appears, however, that these two vortices do not remain distinct further downstream. Instead they seem to interact and shred one another, because at the 90 % plane there are a number of islands of vorticity of complex structure. The contours also indicate the welling up of the vortical layer, coinciding with the thickening of the region of tangled pathlines that we saw in figure 12. The total-pressure contours (figure 13*c*) clearly delineate this region of 50 % loss.

Compared to the coarse solution, the features of the flow here are less diffuse, but they no longer have a laminar character in a small vortical layer over the wing. It is important, however, to point out that outside this layer the flow is smooth and rather similar to that found in the coarse solution, as can be ascertained by comparing the velocity vectors in figures 10 and 12.

### 8.3. *Fine-mesh results*

The final step in our mesh refinement is to halve the cell size in each of the three directions to give the overall dimensions $192\times56\times96$ for just over one million cells. The computations were continued for 2000 time-steps, and all of the data resided in the real memory of the 16 M word CYBER 205 supercomputer. The computational

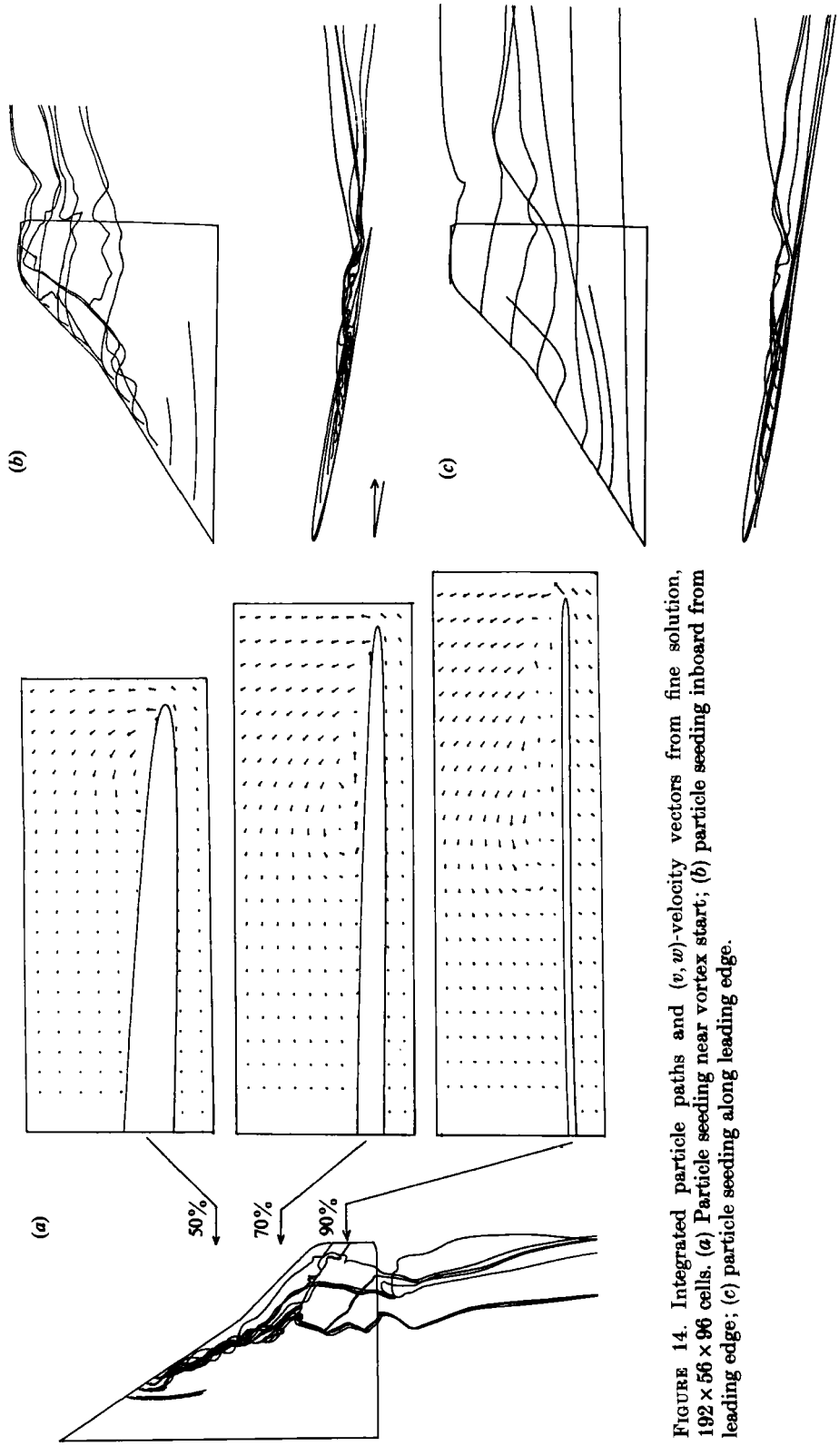


FIGURE 14. Integrated particle paths and $(v, w)$-velocity vectors from fine solution, $192 \times 56 \times 96$ cells. (*a*) Particle seeding near vortex start; (*b*) particle seeding inboard from leading edge; (*c*) particle seeding along leading edge.

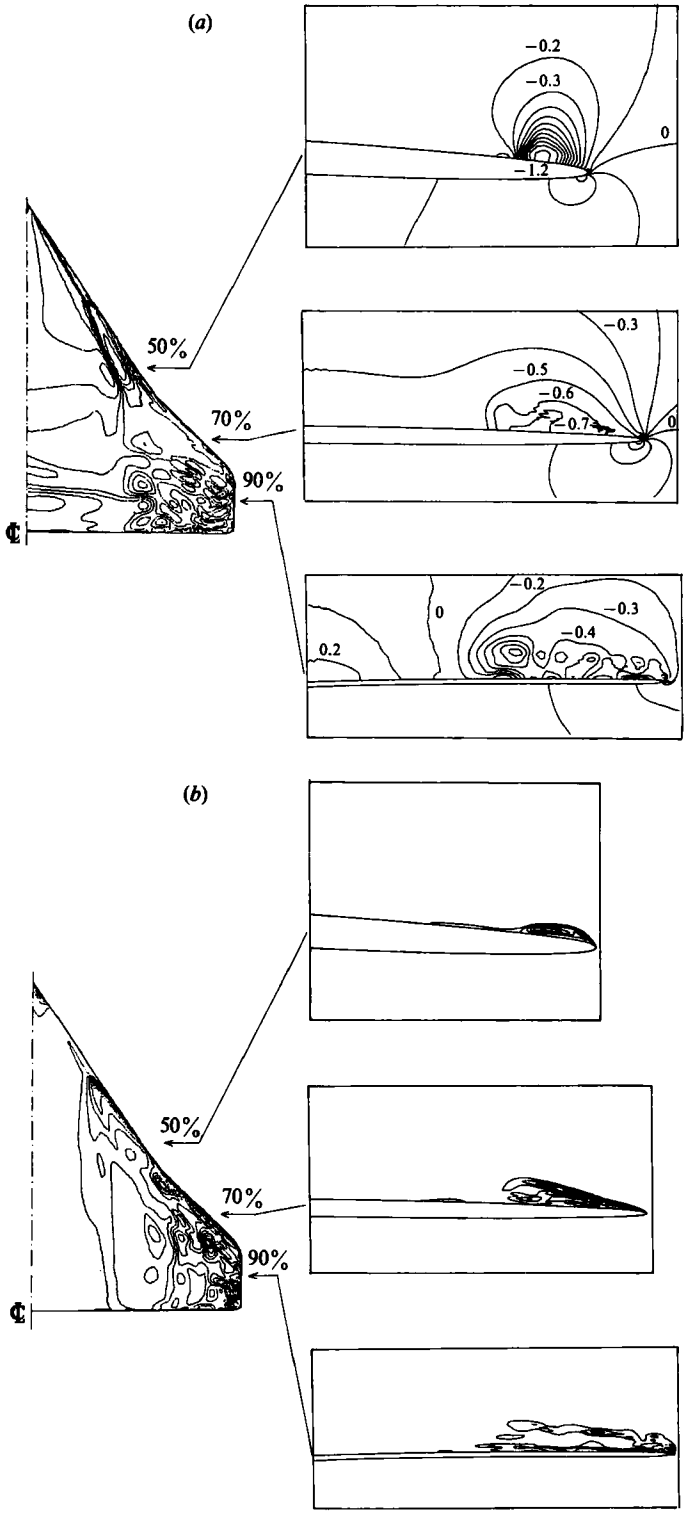


FIGURE 15(*a*, *b*). For caption see facing page.

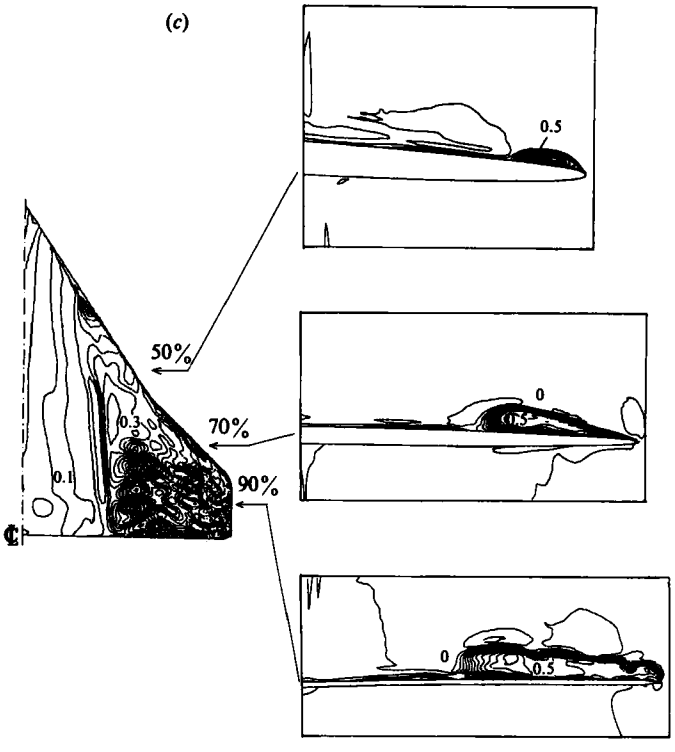


FIGURE 15. Isograms of the solution computed around the cranked delta using the fine $192 \times 56 \times 96$ mesh, $M = 0.9, \alpha = 8°$. (*a*) $C_p$ isobars (increment = 0.1); (*b*) vorticity magnitude (increment 0.005); (*c*) total pressure, $1 - p_t/p_{t_\infty}$ (increment 0.05).

task, which totalled about $2 \times 10^{12}$ arithmetic operations, lasted over 4 CPU hours. The integrated particle paths† are drawn in figure 14. The inboard vortex appears to form at the same location on the leading edge as in the medium solution, but now we see a very dramatic bursting of this coherent vortex at the crank and a shredding into a number of strands (figure 14*a*). The vortical layer lifts upward from the wing as before (figure 14*b*). To demonstrate that this unstable layer is small in extent and sharply delineated from the surrounding laminar flow, we seed our particle paths just a little closer to the leading edge in fig. 14*c* and obtain relatively smooth streamlines.

The pressure contours (figure 15*a*) also attest to the overall wavy nature of the flow in the layer. Compared to the medium results, the cellular structure of the flow on the upper surface is now much more dominant and indicates that as smaller and smaller wavelengths are resolved they grow more and more unstable. The vorticity contours (figure 15*b*) show, however, that the starting position of the vortex, as well as the overall pattern of low pressure inboard of the crank, do not change very much from the medium to the fine solution. What has become clearer in the fine solution is the demarcation line which runs downstream from the vortex starting position and separates the inboard region of laminar flow from the outboard region of disordered motion. The line seems to be the reattachment line of the free shear layer shed from the leading edge since all the flow properties except pressure show a substantial gradient

† Due to the quasi-steady nature of the solution, the streamlines are not strictly steady. It is very likely that they do flap about in the non-smooth region of the vortical layer. The particle paths therefore should be viewed as an instantaneous snapshot of the motion.

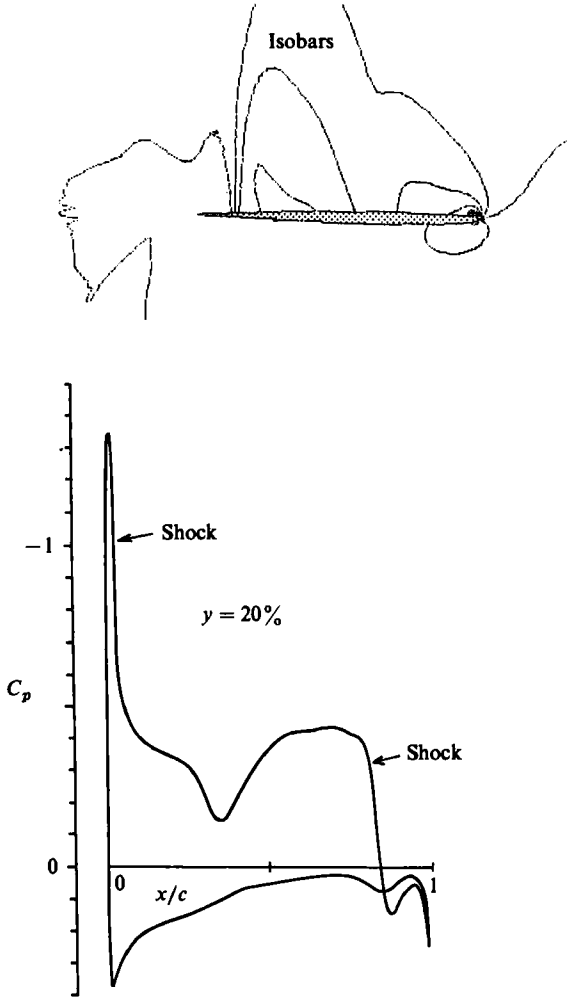


FIGURE 16. Isobars in the plane $y/b = 0.2$, fine-mesh solution.

across it. In the laminar region inboard of this line near the wing root, the recompression found in the coarse solution just ahead of the trailing edge now appears crisply as a weak shock wave with hardly any change in total pressure across it. A stronger shock forms along the leading edge and does produce a substantial loss in total pressure. Figure 16 illustrates this with isobars in the chordwise plane $y/b = 0.2$ along with a plot of the surface $C_p$ values.

These fine-mesh results (figure 15) confirm the trend of the medium results – that the ordered vortex structure undergoes a transition at the crank. A second structure begins to build up again outboard in a narrow band along the leading edge, but the entire region is dominated by the transformation of the coherent inboard vortex into small cellular structures, the result of the bursting at the crank. It seems plausible that the bursting and subsequent shredding into multiple filaments is the result of an instability mechanism. Snow (1978) has found that a three-dimensional disturbance can set off an instability in a vortical flow with a highly sheared azimuthal velocity component. This at least suggests the possibility of a mechanism to transfer

energy from large-scale to small-scale motion, the so-called energy cascade. In a somewhat related situation, Chorin (1982) has studied vortex dynamics and also observed that the vorticity tends to evolve into very non-uniform distributions. As vortices stretch their cross-sections decrease, and the energy associated with them would also increase unless they rearranged themselves in such a way that their velocity fields cancelled. The constraint of energy conservation prevents vorticity from spreading evenly, instead it forces the vortices to fold over on themselves developing into 'tight knots' and hairpin shapes in order to bring about the velocity cancellation.

One significant distinction arises from the comparison of the medium and fine contours. The vorticity has already broken down in the 70% plane of figure 15(*b*) compared to the double-cell pattern of the medium solution (figure 13). Also the chaotic vortical layer is thinner in the 90% plane, and the total-pressure contours (figure 15*c*) reveal the wavy character of the layer. It recalls, in some sense, the flavour of scenario 3 in figure 6.

## 9. Discussion

We have simulated two cases of transonic leading-edge vortex flow and compared the results under mesh refinement. In the case of the pure delta wing, the computations reach a bona fide steady state and the sequence of refined-mesh solutions is converging. The vortex sheet, shed all along the sharp leading edge as a shear layer in the numerical solution, becomes less diffuse, and crisper as portrayed by the total-pressure contours. The roll-up into the core still appears diffuse with probably no more than one turn of the spiral being distinguishable. The total-pressure loss in the core, however, varies little between the medium- and fine-mesh solutions, supporting the explanation of Powell *et al.* (1985) that this depends on the shear at the leading edge and not on the artificial viscosity. The loss of total pressure in the core may be significant for the overall stability of the vortex. Past the trailing edge the flow must compress to the ambient pressure and turn in the direction of the free-stream. The flow in the core slows down and the pressure increases. If the shear, and therefore the total-pressure loss, is great enough, it can happen that the flow stagnates even before attaining free-stream pressure, in which case breakdown seems very likely. This is not the situation for the pure-delta flow presented here; that flow is only slightly disturbed by the trailing edge and remains stable, but it may be significant for the cranked delta with 50% loss.

The other transonic problem considered, the cranked delta wing, produces results that are quite different. Only a quasi-steady solution is reached, and the sequence of refined solutions does not converge to a laminar flow. The most substantial differences between these two cases are the planform of the wing and its detailed geometry. The cranked delta has a round leading edge, but we observe separation in all three mesh solutions. This effect is usually ascribed to the action of artificial viscosity, but we do not see any appreciable shift in the location of the start of the vortex separation, as one might expect with a decrease in artificial viscosity implied in the finer mesh sizes. An alternative conjecture, then, is an inviscid mechanism for the creation of a vortex sheet. The Euler equations embody infinitesimal shear waves, and the question is whether a protruding edge can focus these waves by stretching, cause them to break nonlinearly, and form a vortex sheet (Rizzi 1987*b*). The occurrence of a sheet at the edge would not violate Kelvin's theorem.

We believe that the lack of mesh convergence and the quasi-steadiness of the

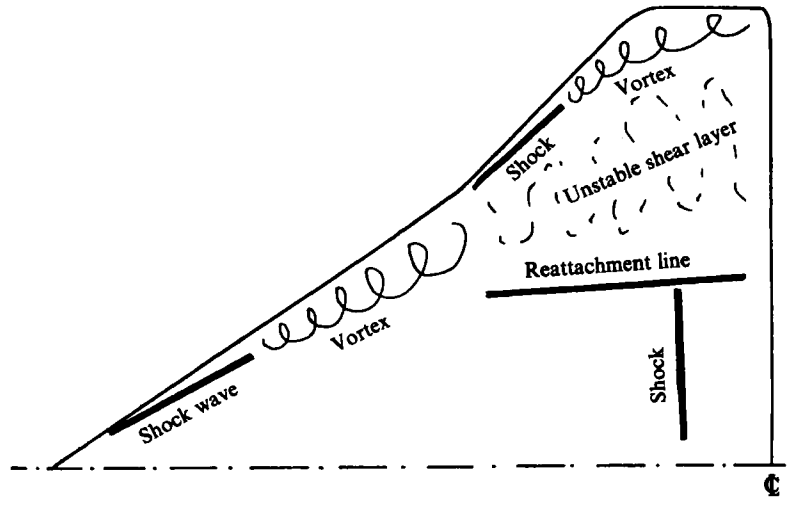


FIGURE 17. Schematic description of the main flow features over the cranked-delta $M_\infty = 0.9$, $\alpha = 8°$.

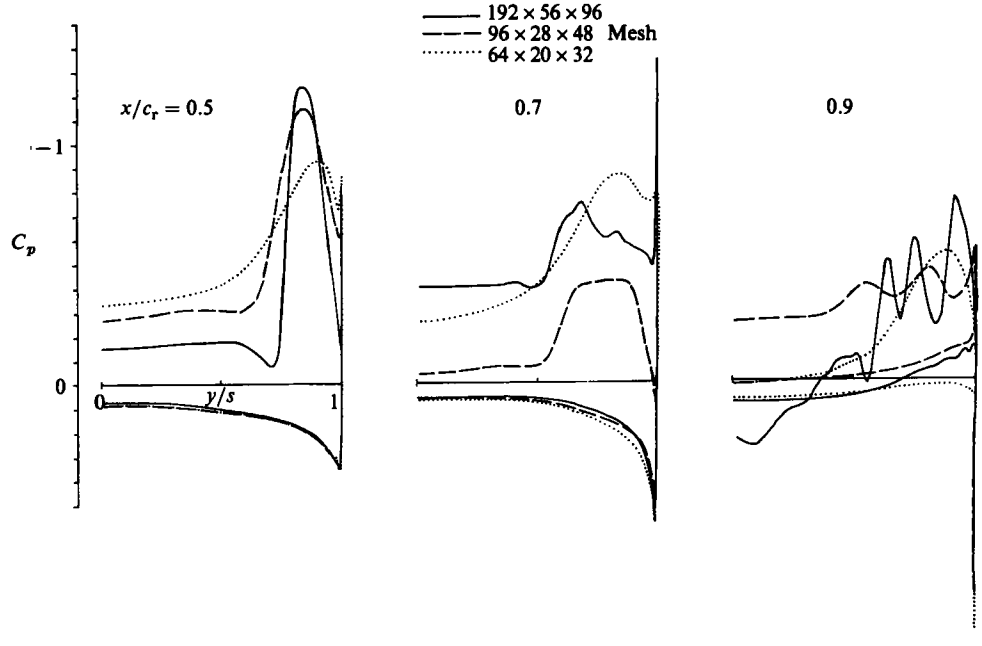


FIGURE 18. Comparison of coarse, medium, and fine results for surface $C_p$ in planes $x/c_r = 0.5$, 0.7, and 0.9.

solution is brought about by the crank in the leading edge. Unlike some earlier investigations of incompressible flow (Thompson 1985) where two distinct and stable vortices appear, our fine-mesh solution portrays the breakdown at the crank of the ordered inboard vortex into a thin but chaotic vortical layer embedded in the otherwise laminar flow over the wing. We suggest that this breakdown is due to a vortical instability. Figure 17 summarizes the main features of the computed flow field. The overall effect of the unstable vortical layer on the wing itself is not

particularly great. Figure 18 compares the coarse-, medium-, and fine-mesh spanwise distribution of surface $C_p$ in the 50 %, 70 %, and 90 % planes, and it shows oscillations in the fine result mainly about the laminar level of pressure, as given by the coarse mesh. It shows good agreement among all three results on the lower surface, and at least broadly comparable pressure levels on the upper surface. The details of the cellular structures are of course different, but the definite transition from the coarse to the medium to the fine results suggests the superposition of these structures upon the broad-scale motion of the coarse results. This comparison supports the suspicion that only a small amount of energy is being drained from the large-scale motion. The lift is not drastically reduced, from $C_L = 0.451$ in the coarse results to 0.442 in the fine results.

## 10. Final remarks

Vortical flows are among the most baffling for the fluid dynamicist to understand. They can develop local regions of extreme velocity and vorticity, they are susceptible to instabilities, and their dynamics are inherently nonlinear. So they are prime subjects for numerical study, particularly when the flow is compressible and mixed with shock waves. Solving the Euler equations by taking differences upon a grid is the technique used. Here, in the spirit of trying to comprehend the results produced by such a method for leading-edge vortex flow, we have focused on two specific problems designed to highlight some of the outstanding uncertainties involved with this approach, like inviscid separation, loss in total pressure, the numerical capturing of vortex sheets, and the overall dynamics and stability of the vortical structures in the flow. The first problem is one of classical vortex flow around a pure delta wing, about which much already is understood. It sets the stage for the second case, vortex flow around a twisted delta wing for which less is known. The *bête noire* of the mesh-based computational approach is the artificial diffusion of the flow features due to numerical dissipation. In order to gauge this unwanted effect, we have carried out the solutions to both problems using a series of progressively refined meshes up to just over one million cells. In the solution to the pure-delta problem we observed that a shear layer was shed from the leading edge and rolled up to form a vortex, much as one would expect qualitatively in incompressible flow. The results converged under mesh refinement to a laminar and stable flow with a relatively thin shed shear layer but a relatively diffuse core in the fine-mesh solution.

In the results to the second problem we observed separation from the round leading edge of a cranked delta wing at transonic speed. The shed layer develops into a vortex that bursts and shreds at the crank and evolves into a thin chaotic vortical layer superposed upon a laminar flow field. It seems likely that the cause of the breakdown is a Rayleigh-type instability. The computed results are only quasi-steady in time, and are not converging with mesh refinement as the first problem did. The structures within it become crisper, and the vortical layer itself becomes thinner as the mesh is refined. Whether further mesh refinement brings convergence or whether this trend continues so that even smaller scales appear and the layer grows even thinner are still matters of speculation. The central issue, and a controversial one, is whether, using a mesh-based approach, we can hope to simulate a flow containing vortical instability with some degree of validity. Our guess is that although the precise details computed within the unstable layer may be false, the method can predict the onset of the instability and the gross motion of the layer.

We wish to thank Dr E. Lojacono of Aeritalia, Torino, for suggesting the cranked-delta configuration to us, Peter Eliasson of FFA for helping us to draw the fluid pathlines, and Control Data for offering us the computer time to run the calculations. We are also grateful to Professor E. Murman of MIT for his many helpful discussions.

## REFERENCES

BETCHOV, R. 1965 On the curvature and torsion of an isolated vortex filament. *J. Fluid Mech.* **22**, 471–479.

BRENNENSTUHL, U. & HUMMEL, D. 1982 Vortex formation over double-delta-wings. *ICAS Paper*, 82–6.6.3.

CHORIN, A. J. 1982 The evolution of a turbulent vortex. *Commun. Math. Phys.* **83**, 517–535.

ERIKSSON, L. E. 1982 Generation of boundary-conforming grids around wing–body configurations using transfinite interpolation. *AIAA J.* **20**, 1313–1320.

FORNASIER, L. & RIZZI, A. 1985 Comparisons of results from a panel method and an Euler code for cranked delta wing. *AIAA Paper* 85-4091.

HALL, M. G. 1972 Vortex breakdown. *Ann. Rev. Fluid Mech.* **4**, 195–218.

HIRSCHEL, E. H. & FORNASIER, L. 1984 Flowfield and vorticity distribution near wing trailing edges. *AIAA paper* 84-0421.

HOEIJMAKERS, H. W. M. 1983 Numerical computation of vortical flows about wings. *NLR Rep.* MP 83073 U, Nat. Aero. Lab., Amsterdam.

HOEIJMAKERS, H. W. M. & RIZZI, A. 1984 Vortex-fitted potential solution compared with vortex-captured Euler solution for delta wing with leading edge vortex separation. *AIAA Paper* 84-2144.

HOEIJMAKERS, H. W. M. & VAATSTRA, W. 1983 A higher-order panel method applied to vortex sheet roll-up. *AIAA J.* **21**, 516–523.

HOEIJMAKERS, H. W. M., VAATSTRA, W. & VERHAAGEN, N. G. 1983 On the vortex flow over delta and double-delta wings. *J. Aircraft* **20**, 825–832.

KRAUSE, E., SHI, X. G. & HARTWICH, P. M. 1983 Computation of leading-edge vortices. *AIAA Paper* 83-1907.

LEIBOVICH, S. 1978 The structure of vortex breakdown. *Ann. Rev. Fluid Mech.* **10**, 221–246.

MOORE, D. W. & GRIFFITH-JONES, R. 1974 The stability of an expanding circular vortex sheet. *Mathematika* **21**, 128–133.

MOORE, D. W. 1973 The stability of an evolving two-dimensional vortex sheet. *Mathematika* **23**, 35–44.

MURMAN, E. M. & RIZZI, A. 1986 Applications of Euler equations to sharp edge delta wings with leading edge vortices. In *Proc. AGARD Sym. Appl. Comp. Fluid Dyn. Aero., AGARD-CP-412.*

MURMAN, E., RIZZI, A. & POWELL, K. 1985 High resolution solutions of the Euler equations for vortex flows. In *Progress and Supercomputing in Computational Fluid Dynamics* (ed. S. Abarbanel & E. Murman), pp. 93–113. Boston: Birkhauser.

POWELL, K., MURMAN, E., PEREZ, E. & BARON, J. 1985 Total pressure loss in vortical solutions of the conical Euler equations. *AIAA Paper* 85-1701.

RIZZI, A. 1982 Damped Euler-equation method to compute transonic flow around wing–body combinations. *AIAA J.* **20**, 1321–1328.

RIZZI, A. 1985*a* Euler solutions of transonic vortex flows around the Dillner wing. *J. Aircraft* **22**, 325–328.

RIZZI, A. 1985*b* Modelling vortex flowfields by supercomputers with super-size memory. *Aero J.* **89**, 149–161.

RIZZI, A. 1987*a* Multi-cell vortices observed in fine-mesh solutions to the incompressible Euler equations. In *Super Computers and Fluid Dynamics* (ed. K. Kuwahara). Lecture Notes in Engineering. Springer.

RIZZI, A. 1987*b* Separation phenomena in 2D and 3D numerical solutions of the Euler equations. In *Proc. 7th INRIA Conf. Computing Methods in Appl. Sci. Engng* (ed. R. Glowinski *et al.*). North-Holland.

RIZZI, A. & BAILEY, H. E. 1976 Finite volume solution of the Euler equations for steady three-dimensional transonic flow. In *Proc. 5th Intl Conf. Num. Methods Fluid Dyn.* (ed. A. I. van der Vooren & P. J. Zandbergen). Lecture Notes in Physics, vol. 59, pp. 347–357. Springer.

RIZZI, A. & ERIKSSON, L. E. 1984 Computation of flow around wings based on the Euler equations. *J. Fluid Mech.* **148**, 45–71.

RIZZI, A. & ERIKSSON, L. E. 1985 Computation of inviscid incompressible flow with rotation. *J. Fluid Mech.* **153**, 275–312.

RIZZI, A. & PURCELL, C. J. 1986*a* Vortex-stretched flow around a cranked delta wing. *J. Aircraft* **23**, 636–640.

RIZZI, A. & PURCELL, C. J. 1986*b* Disordered vortex flow computed around a cranked delta wing at subsonic speed and high incidence. *ICAS Paper* No. 86-1.4.1.

SMITH, J. H. B. 1984 Theoretical modelling of three-dimensional vortex flows in aerodynamics. *Aero J.*, April 1984, 101–116.

SMITH, J. H. B. 1985 Numerical solutions for three-dimensional cases – delta wings. In *Test Cases for Inviscid Flow Field Methods. AGARD* AR-211.

SNOW, J. T. 1978 On inertial instability as related to the multiple-vortex phenomenon. *J. Atmos. Sci.* **35**, 1660–1677.

THOMPSON, D. H. 1985 A visualization study of the vortex flow around double-delta wings. *ARL-AERO-R-165*, Melbourne.